AN APPROACH TO OPTIMUM LOADING OF A SOLAR ARRAY WHICH EXPERIENCES TEMPERATURE CHANGES

A Thesis

Presented to

the Faculty of the School of Engineering and Applied Science

University of Virginia

In Partial Fulfillment

of the Requirements for the Degree

Master of Electrical Engineering

by

Merton Sussman

March 1968

APPROVAL SHEET

This thesis is submitted in partial fulfillment of

the requirements for the degree of

Master of Electrical Engineering

Merton Sussman

Author

Approved:

Faculty Advisor

Dean, School of Engineering and
Applied Science

March 1968

ACKNOWLEDGMENT

The author wishes to thank Dr. Mark Foster for his constructive criticisms and encouragement while serving as advisor during the preparation of this thesis. Appreciation is expressed to the administrative personnel of the National Aeronautics and Space Administration, Spacecraft Power System Section, for their cooperation in the execution of this work. A special acknowledgment is given to Mr. John L. Patterson, section head of the Spacecraft Power System Section, for his continuous encouragement and support in the preparation of this thesis. Appreciation is given to the Langley Research Center for permitting this study to be submitted as a thesis.

TABLE OF CONTENTS

CHAPTER		PAGE
I.	INTRODUCTION AND PHILOSOPHY	1
II.	MISSION CONSTRAINTS	6
	Critical Orbit Defined	6
	Type of Solar Cell Chosen	8
	Experiment Power Demand	10
	Orbit Mission Lifetime	10
III.	CONSTANT-CURRENT BATTERY-CHARGE SYSTEM	11
	Battery Characteristics	11
	Solar Array Size Determined	18
IV.	TAPER-CURRENT BATTERY-CHARGE SYSTEM	26
	Battery Taper-Charge Current Philosophy	30
	Battery Taper-Charge Current - Trial I	31
	Sizing Up the Solar Array - Trial I	36
	Battery Taper-Charge Current - Trial II	43
	Sizing Up the Solar Array - Trial II	43
	Solar Array Characteristics for TCS	45
V.	COMPARISON BETWEEN CCS AND TCS	51
VI.	TAPER-CURRENT BATTERY-CHARGE SYSTEM CANDIDATE	54
VII.	EXPERIMENTAL RESULTS	58
VIII.	CONCLUSIONS	68
BIBLIOGRAPHY		71
APPENDIX I		73

LIST OF FIGURES AND TABLE

FIGURE PAGE

1. Solar Array Temperature and Illumination Intensity vs Orbit Time During Critical Orbit 7
2. Normalized Solar Cell Data vs Solar Cell Temperature . . 9
3. Block Diagram of Constant-Current Battery-Charge System 12
4. Efficiency of Voltage Regulator vs Regulator Input Voltage for Constant-Current Battery-Charge System . . 14
5. Battery Charge and Discharge Voltage vs Residual Battery Charge for Constant-Current Battery-Charge System 17
6. Solar Array Characteristics for Constant-Current Battery-Charge System 21
7. Battery Charge Voltage vs Array Temperature for Constant-Current Battery-Charge System 24
8. Block Diagram of Taper-Current Battery-Charge System . . 27
9. Assumed Contour of Taper Battery-Charge Current vs Illumination Interval 32
10. Efficiency of Voltage Regulator vs Battery Voltage for Taper-Current Battery-Charge System 34
11. Efficiency of Taper Control Circuit vs Solar Array Voltage 35
12. Battery Charge Voltage vs Residual Battery Charge for Taper-Current Battery-Charge System 40

FIGURE PAGE

13. Battery Charge Voltage vs Array Temperature for Taper-Current Battery-Charge System 41

14. Battery Taper Charge Current Resulting from Trial I . . . 42

15. Battery Taper Charge Current Resulting from Trial II . . 46

16. Solar Array Characteristics for Taper-Current Battery-Charge System 47

17. Duty Cycle vs Array Temperature 50

18. A Candidate for the Taper-Current Battery Charge System 55

19. Test Set-Up Utilized to Obtain Solar Array Simulator Reference Curves 60

20. Solar Array Simulator Reference Curves 61

21. Block Diagram of Test Set-Up for Empirical Data of Taper-Current Battery-Charge System 62

22. Duty Cycle (Measured) vs Open Circuit Voltage for Taper-Current Battery-Charge System 65

23. Duty Cycle (Calculated) vs Open Circuit Voltage for Taper-Current Battery-Charge System 67

(A-1) Duty Cycle Derivation Sketch 73

TABLE

I. Empirical Data for Taper-Current Battery-Charge System . . 64

LIST OF SYMBOLS

A	solar array area
C	solar array cost
CCS	constant-current battery-charge system
D-D	percent depth of battery discharge
EFF_B	battery charge-discharge efficiency
EFF_R	efficiency of voltage regulator
EFF_T	efficiency of taper charge control circuit
f_S	switching frequency of taper charge control circuit
I	illumination intensity
I_{B_D}	battery discharge current
I_{B_K}	constant current battery charging value
I_{B_T}	battery taper charge current
$I_{B_{T_{max}}}$	maximum battery taper charge current
$I_{B_{T_{min}}}$	minimum battery taper charge current
I_{IN}	solar array terminal current
I_L	experiment current demand
I_l	solar array simulator terminal current
I_p	solar array current at maximum available power
i_p	current per solar cell at maximum available power
i_{sc}	short circuit current per solar cell
Ni-Cd	nickel-cadmium battery

N_p	number of parallel strings of solar cells
N_S	number of series connected solar cells
N_T	total number of solar cells comprising the solar array
P_A	maximum available solar array power
P_{IN}	solar array terminal power
P_L	experiment power demand
P_S	power capacity of the solar array at maximum array temperature
p_A	maximum available power per solar cell
T_A	solar array temperature
TCC	taper charge control circuit
TCS	taper-current battery-charge system
T_D	dark interval of orbit
$T_{D_{max}}$	maximum dark interval
T_L	illumination interval of orbit
$T_{L_{min}}$	minimum illumination interval
T_{ON}	"on time" of duty cycle switch
T_S	switching period of duty cycle switch
t	interval of time during orbit
v_{oc}	open circuit voltage per solar cell
v_p	voltage per solar cell at maximum available power
V_{B_C}	battery charging voltage
V_{B_D}	battery discharge voltage
V_{B_p}	plateau discharge battery voltage
V_{IN}	solar array terminal voltage

V_L	experiment regulated voltage
V_t	solar array simulator terminal voltage
V_P	voltage at maximum available power for entire solar array
V_R	voltage regulator input voltage
V_T	dc voltage simulating solar array temperature sensor signal
WT	solar array weight
τ	duty cycle of taper charge control circuit
ξ_{B_C}	quantity of charge during the illumination orbit interval
ξ_{B_R}	residual battery charge during orbit
ξ_C	nominal battery discharge capacity
V_{OC}	solar array terminal open circuit voltage

ABSTRACT

A method is described and an example given of how the utilization of a solar array can be optimized. The method consists of choosing an earth-orbiting spacecraft mission and assigning to the mission various environmental and experimental power constraints. Spacecraft power requirements are provided by a solar array. A storage battery stores energy for use during the nonilluminated portion of the orbit. The required solar array is first determined on the basis of a constant-current battery-charging system and then on the basis of a taper-current battery-charging system. It is shown the taper current-charging system results in improved solar array utilization. This conclusion is reached since the solar array, obtained by taper current-charging, is smaller in area, lighter in weight, and less expensive than the constant-current charge array. Taper-current battery-charging is shown to be possible by controlling the operating point of the solar array. The operating point is controlled in a continuous manner versus array temperature and in a digital manner versus experiment power demand.

CHAPTER I

INTRODUCTION AND PHILOSOPHY

A solar array generally consists of many series and parallel combinations of solar cells. A solar cell is a solid-state, two-terminal device, which converts illumination energy into electrical energy. The available electrical power from an individual solar cell is small, nominally 25 milliwatts at 425 millivolts. By connecting many solar cells in series, the available power and voltage are increased. By paralleling many series connected strings of solar cells, the available current is increased.

The National Aeronautics and Space Administration has in the past and will continue in the future to utilize the solar array on spacecraft orbit and probe missions. During spacecraft flight, a portion of the sun's illumination falls on the spacecraft solar array. The solar array converts this intercepted illumination energy into electrical energy to power the various spacecraft experiments. During each mission there will be intervals of time in which the solar array will not receive any illumination energy from the sun. For example in an earth-orbital spacecraft mission, there will always be an interval of time when the earth will block the solar array from the illumination energy of the sun. This interval is known as the dark or nonilluminated portion of the orbit. Generally it is desirable for the spacecraft experiments to operate continuously throughout

each earth orbit. In order to fulfill this requirement, it is necessary to power the experiments from another energy source during the dark portion of the orbit.

The typical solar array spacecraft power system consists of a solar array, a centralized voltage regulator, a storage battery, and the various experiment loads. During the illuminated portion of the earth orbit, the solar array powers the experiments and charges the storage battery. During the dark portion of the orbit, the storage battery powers the experiments. Occasionally the storage battery is also utilized during the illuminated portion of the orbit to aid the solar array in powering experiments during the peak power demand. The nickel-cadmium battery is utilized most often as the spacecraft storage battery, primarily due to the large number of possible recharge cycles, as well as ruggedness and reliability. A silver-zinc storage battery is sometimes used when battery energy density is extremely important. A silver-zinc battery will not tolerate as many recharge cycles as the nickel-cadmium battery, hence, would generally be utilized on short duration orbital missions.

When a sufficiently large solar array is provided to carry its load under worst temperature conditions, the essence of the design is to generate as little heat as possible. Therefore, power system efficiency is very important. High efficiency results in fewer heating problems among the various circuit components, thereby, helping to assure system reliability. Nondissipative (i.e. switching)

voltage regulators are more efficient than the dissipative types. However, the nondissipative regulators produce greater radio-frequency interference and ripple. Usually efficiency is the more important parameter, so the nondissipative type is chosen. In practice the efficiency of the nondissipative regulator is from 10 to 20 per cent higher than that of the dissipative type.

It is desirable to minimize spacecraft power system weight. Such minimization saves propulsion power thus saving costs in spacecraft research programs. The largest and heaviest subassembly in the spacecraft power system is the solar array hence it is desirable to minimize its size and weight. This thesis attempts to show how a solar array can be utilized in an optimum manner. An optimum array is defined as the smallest, lowest weight, and least expensive solar array for a given spacecraft mission. This analysis is done by choosing a sun oriented earth orbiting spacecraft mission. A representative, critical earth orbit is described. The experiment power requirements and the solar array temperature range are similarly postulated as representative of practice. For the same mission constraints, the required solar array size is determined on the basis of two different systems. These systems are a constant-current battery-charge system, and a taper-current battery-charge system. In this analysis the same type of storage battery is utilized for each of the two different systems. Hence, the analysis is essentially a comparison of the required solar arrays of the two systems.

The constant-current battery-charge system is based on the idea of charging the storage battery at a constant current during the entire illuminated orbit period. The battery discharge energy is calculated during the dark portion of the critical orbit. The required battery-charge energy exceeds the discharge energy, due to the charge-discharge efficiency factor of the battery. The size of the solar array is determined under conditions of maximum experiment power demand and maximum array temperature during the critical orbit.

The taper-current battery-charge system controls the value of battery charging current by controlling the operating point of the solar array. The solar array size is determined under conditions of maximum experiment power demand and maximum expected array temperature during the critical orbit. The system is so arranged that as long as the experiment power demand remains at its maximum value, the duty cycle of the taper control circuit forces the solar array to operate at its point of maximum power transfer. Hence as the array temperature varies, the duty cycle varies to force the array operating point to track the maximum power locus. However, when the battery is considered fully charged, the duty cycle function shifts to one that will just carry the experiment load. For this thesis analysis, only two experiment power levels are considered possible.

The taper-current battery-charging method is of an iterative nature. As the first trial in the method, a linear taper charge contour is assumed. The discrepancy between the assumed and actual

battery taper charge contour is noted, and a correction factor is inserted in the second trial. For the example described only two trails were necessary to obtain the required battery-charging energy.

CHAPTER II

MISSION CONSTRAINTS

In this chapter several mission constraints are discussed. It is to be understood that the same constraints are imposed on each of the two power systems.

Critical Orbit Defined

The interval of time required for the orbiting spacecraft to travel once around the earth is the orbiting period. For the majority of earth-orbiting missions, the orbiting period remains constant during the orbiting phase of the mission (its "orbital life"). The portion of the orbiting period that the solar array is under illumination is termed the illuminated time. The illuminated time will usually vary between a minimum and a maximum value during the orbital life of the spacecraft. In fact the illuminated time could become equal to the orbiting period, which is the continuous sunlight mode. The interval during which the solar array is under illumination for the minimum illuminated time is known as the critical period. During the critical period the dark portion of the orbit is at its maximum value. This orbit configuration is termed critical in that the battery must be given sufficient charge during the shortest interval of time to allow for discharge during the longest interval of time.

The same critical period is chosen for each of the compared systems and is described in Figure 1. The critical period is

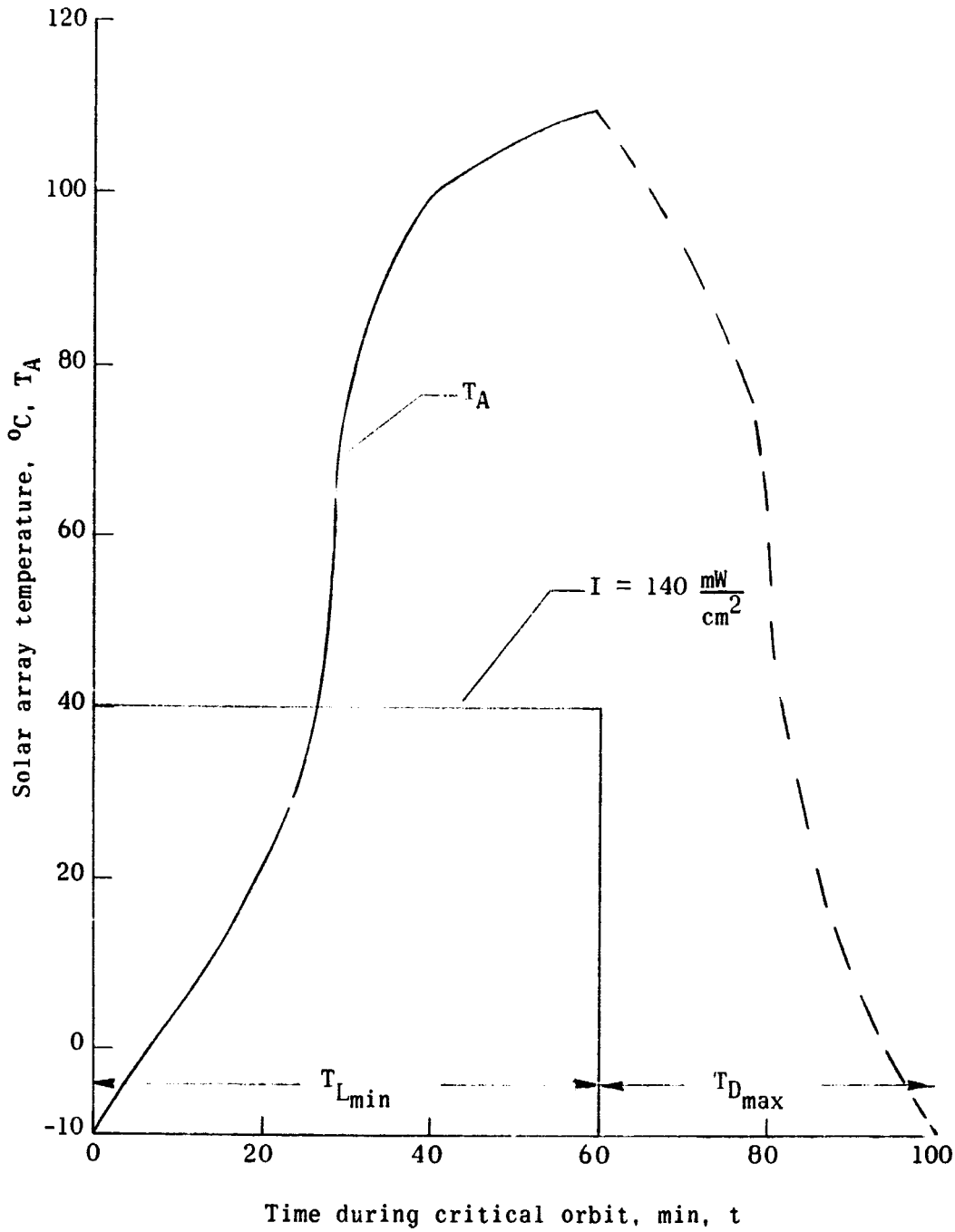

Figure 1.- Solar array temperature and illumination intensity vs. orbit time during critical orbit.

100 minutes, the minimum illuminated interval is 60 minutes, and the maximum dark time is 40 minutes. Each of the two analyzed systems has the same range of solar array temperature, which is from -10° C to +110° C. From Figure 1, note that the illumination is constant during the illuminated portion of the period. For this thesis analysis, we will consider the orbiting spacecraft to be of the sun-oriented type. A sun-oriented solar array has essentially a constant illumination during the illuminated portion of the orbit. A spinning orbiting spacecraft continues to spin about its axis and results in a ripple superimposed on the illumination function.

Type of Solar Cell Chosen

Figure 2 represents normalized solar cell data of short circuit current, open circuit voltage, maximum available power, voltage at maximum available power, and current at maximum available power versus solar cell temperature. The data in this figure are for a ten (10) cell average of type N120CG solar cells. Figure 2 was obtained from extrapolating manufacturing data.[1] The original manufacturer's data indicated this data from -10° C to +70° C. The extrapolation was done by assuming the general slopes of each of the curves at +70° C to remain fairly constant up to +110° C. According to the solar array engineer, Mr. Walter E. Ellis, of the Spacecraft Power System Section, this is a good assumption. For this analysis, each

---

[1] "Solar Cells for Spacecraft Power Systems," Dr. Bernard Ross, Hoffman Electronics Corporation, March 1963.

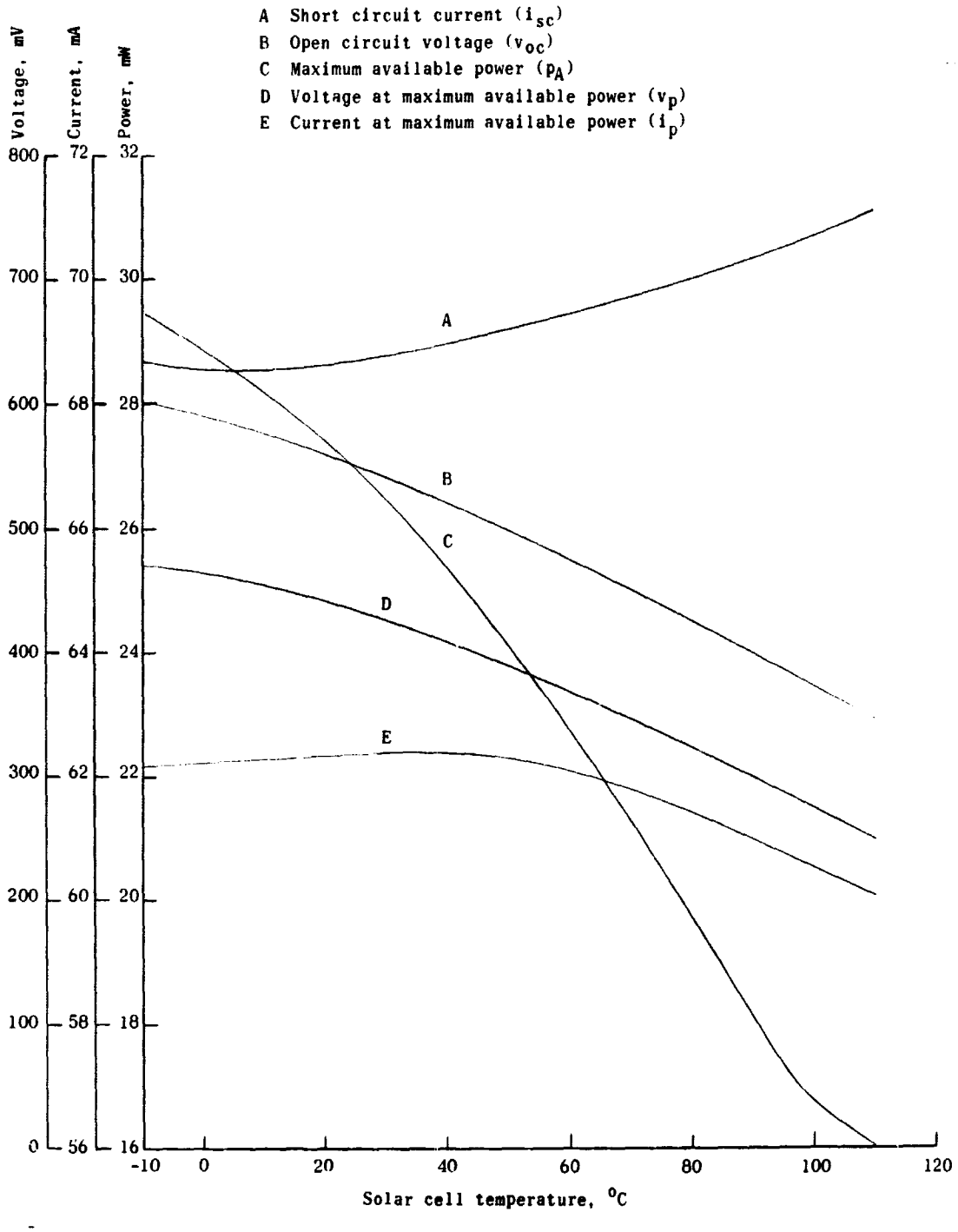

Figure 2.- Normalized solar cell data vs. solar cell temperature.

of the two power systems has its solar array consisting entirely of N120CG solar cells. Hence Figure 2 is used as a basis of solar array design for both power systems. Note in Figure 2 that the maximum available power decreases as solar cell temperature increases. Hence, in determining the size of each solar array, the maximum solar array temperature will be the critical temperature.

Experiment Power Demand

For this comparative analysis only two experiment power demands will be considered. The experiment power demand (P_L) can either be at its maximum value $(P_{L_{max}})$ of 56.0 w or at its lower value $(P_{L_{min}})$ of 28.0 w. Since an experiment regulated voltage (V_L) of 28.0 vdc is fairly common for spacecraft loads, it was chosen. Hence, the experiment load current (I_L) is either 2.0 amp or 1.0 amp. Naturally the size of the solar array for each of the two systems will be based on $P_{L_{max}}$.

Orbit Mission Lifetime

The intended earth orbit mission lifetime is 2 years for each system. Since T is 100 minutes, the total number of lifetime orbits is 10,500. This represents an appreciable number of charge-discharge cycles, hence, a nickel-cadmium storage battery is chosen for each system.

CHAPTER III

CONSTANT-CURRENT BATTERY-CHARGE SYSTEM

This chapter analyzes the constant-current battery-charge system (CCS). In this chapter the storage battery, that will be utilized for both the CCS and the taper-current battery-charge system (TCS), will be chosen. After discussing the battery discharge and charge requirements, the size of the solar array is determined under conditions of $P_{L_{max}}$ and $T_{A_{max}}$ during T_C.

Figure 3 represents the basic block diagram of the CCS. In an actual practical system, switches S_1 and S_2 would each be electronic rather than mechanical. During the illumination interval (T_L) S_1 remains closed while S_2 remains open. The solar array feeds power to the voltage regulator. One output of the regulator powers the spacecraft experiments, and the other output charges the nickel-cadmium (Ni-Cd) battery. During the dark interval (T_D) S_1 remains open and S_2 remains closed. The Ni-Cd battery discharges into the voltage regulator, which in turn powers the experiments.

Battery Characteristics

In order to define the Ni-Cd battery-charge requirements during T_L, it is first necessary to discuss the discharge characteristic during T_D. The nominal discharge plateau voltage of a Ni-Cd storage cell is 1.23 vdc. Let the Ni-Cd battery consist of 24 series connected cells, that is, a nominal plateau discharge voltage (V_{B_p}) of 29.5 vdc.

NOTE: s_1 **remains closed during entire illumination interval and remains open during entire dark interval**

s_2 **remains closed during entire dark interval and open during entire illumination interval**

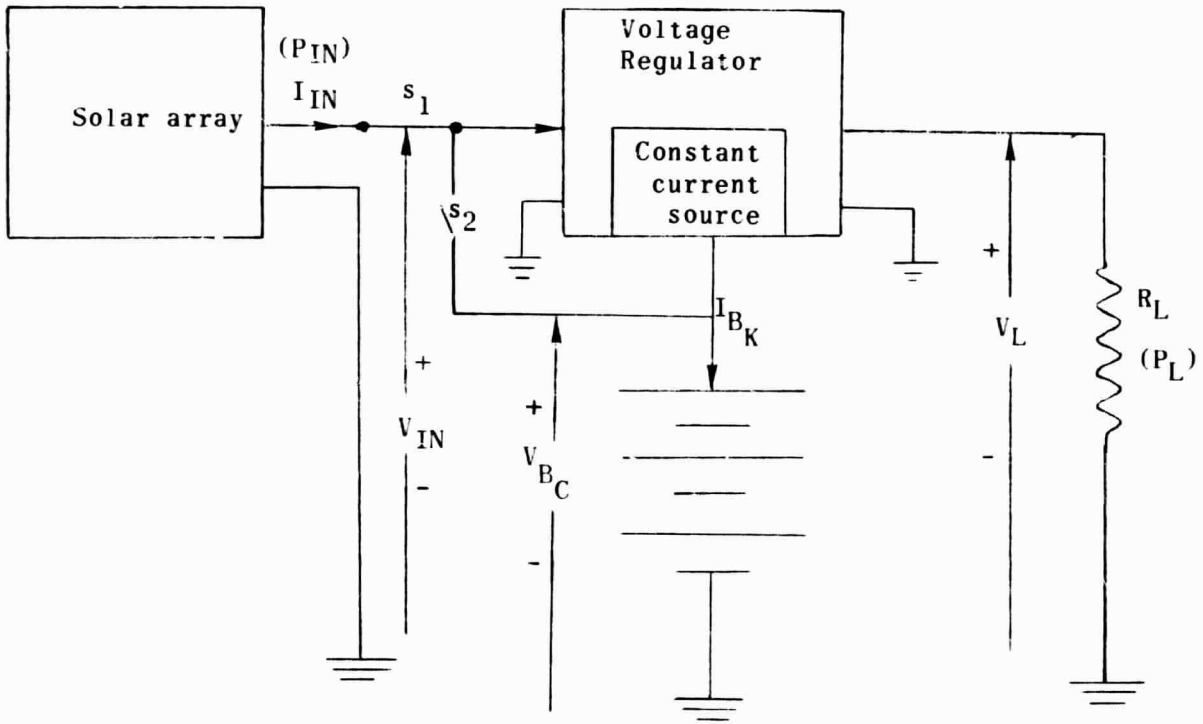

Figure 3.- Block diagram of constant-current battery-charge system.

Figure 4 represents the efficiency of the voltage regulator $\left(EFF_R\right)$ versus the input regulator voltage $\left(V_R\right)$ for $P_{L_{max}}$ and $P_{L_{min}}$. Although Figure 4 was arbitrarilly constructed, it does reflect nondissipative regulator efficiency performance.

The Ni-Cd battery discharge current $\left(I_{B_D}\right)$ can be expressed as shown in Equation (1)

$$I_{B_D} = \frac{P_L}{\left(EFF_R\right)\left(V_{B_D}\right)} \tag{1}$$

During actual orbital missions, V_{B_D} varies approximately 10 per cent. This small variation causes only a small change in EFF_R (nominally 5 per cent); hence, the variation in I_{B_D} will be small (nominally 5 per cent). For purposes of the calculation of battery discharge, let us select a V_{B_p} = 29.5 vdc and assume it remains constant. From Figure 4, EFF_R = 0.95 since $P_{L_{max}}$ = 56 w is under concern. Hence, from Equation (1), I_{B_D} = 2.0 amp. Since the battery discharge voltage is taker as constant (29.5 vdc), the I_{B_D} is taken as constant (2.0 amp) during the dark interval of the orbiting period.

During the dark interval of the orbiting period, the battery releases (discharges) a total quantity of charge that can be described as:

$$\xi_{B_D} = \int_o^{T_D} i_{B_D}\, dt \tag{2}$$

where:

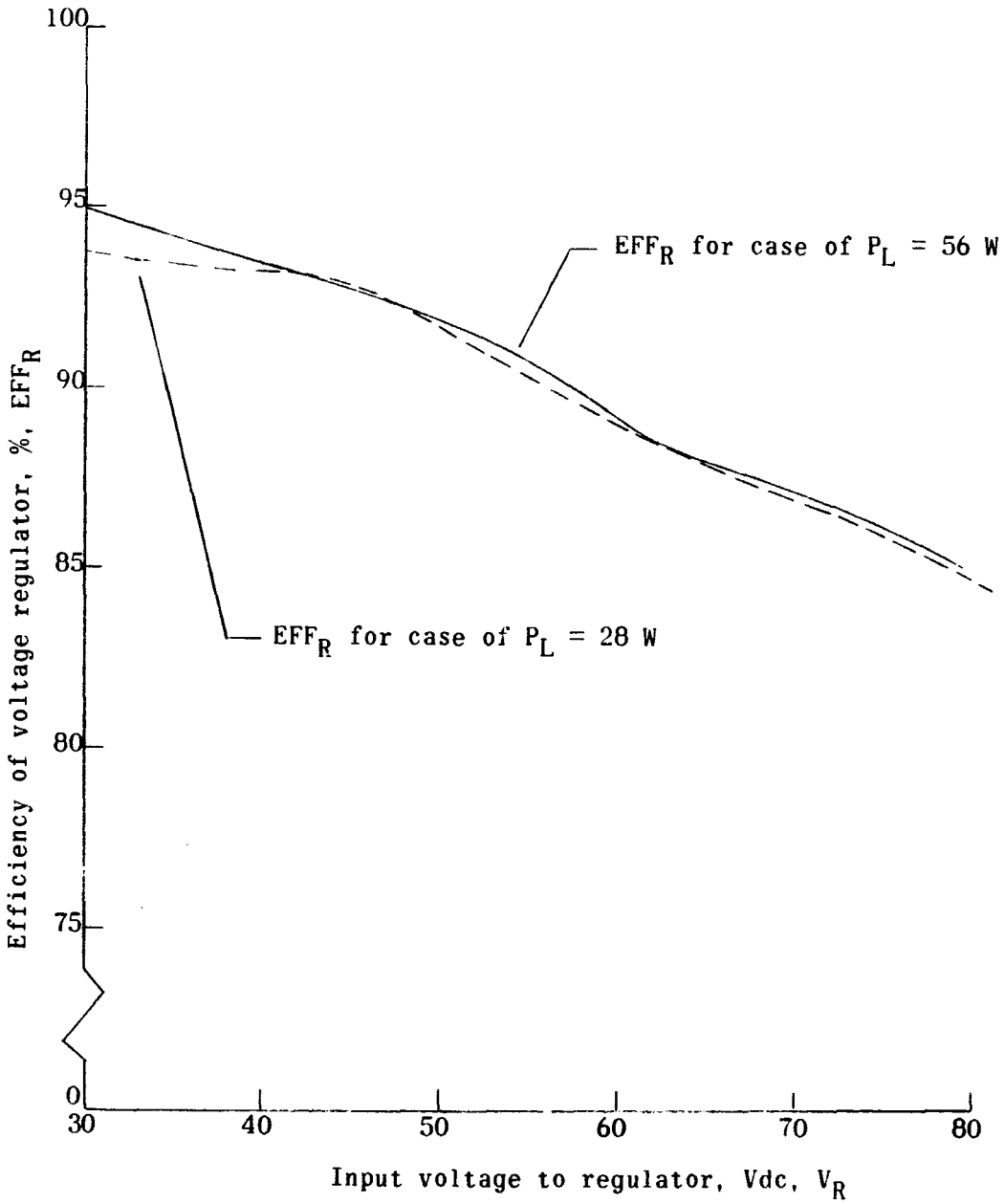

Figure 4.- Efficiency of voltage regulator vs. regulator input voltage for constant-current battery-charge system.

ξ_{B_D} is the total quantity of charge that is discharged from the battery during the dark interval.

T_D is the dark interval, and

i_{B_D} is the, generally, varying battery discharge current during the dark interval.

If it is assumed that the battery discharge current remains constant, then the total quantity of charge released from the battery during the dark interval can be expressed as

$$\xi_{B_D} = \left(I_{B_D}\right)\left(T_{D_{max}}\right) \tag{3}$$

where $T_{D_{max}}$ represents the longest dark interval (i.e., critical orbit case).

For values of $I_{B_D} = 2.0$ amp and $T_{D_{max}} = 0.67$ hr, Equation (3) gives the value of 1.33 A-hr. It seems reasonable to choose a Ni-Cd battery with a nominal discharge capacity of 6.0 A-hr. The relationship between battery discharge capacity $\left(\xi_C\right)$, amount of battery discharge $\left(\xi_{B_D}\right)$, and per cent depth of battery discharge (D-D) is:

$$\text{D-D} = \frac{\xi_{B_D}}{\xi_C} \times 100 \tag{4}$$

For the conditions of $\xi_{B_D} = 1.33$ A-hr and $\xi_C = 6.0$ A-hr, Equation (4) gives a D-D = 22.2 per cent.

During the minimum illuminated interval enough charge must be supplied to the 6.0 A-hr Ni-Cd battery to satisfy the discharge and battery loss requirements. The battery charge-discharge efficiency

$\left(EFF_B\right)$ is a ratio of the total output charge (discharge) to the total input charge (charge) of a battery. The $\left(EFF_B\right)$ during an actual orbital mission may vary ±5 per cent; however, a nominal EFF_B, for a Ni-Cd battery is 80 per cent.[2]

The total required battery charge $\left(\xi_{B_C}\right)$ can be stated as:

$$\xi_{B_C} = \frac{\xi_{B_D}}{EFF_B} \tag{5}$$

For values of $\xi_{B_D} = 1.33$ A-hr and $EFF_B = 0.80$, Equation (5) gives

$$\xi_{B_C} = 1.66 \text{ A-hr}$$

the cyclic residual battery charge[3] $\left(\xi_{B_R}\right)$ will vary, during the critical orbit, from 6.0 A-hr to 4.67 A-hr during $T_{D_{max}}$ and from 4.34 A-hr to 6.0 A-hr during the minimum illuminated time.

The required constant battery charging current $\left(I_{B_K}\right)$ during $T_{L_{min}}$ is easily found since:

$$I_{B_K} = \frac{\xi_{B_C}}{T_{L_{min}}} \tag{6}$$

For values of $\xi_{B_C} = 1.66$ A-hr and $T_{L_{min}} = 1.0$ hr, $I_{B_K} = 1.66$ amp.

Figure 5 shows one cycle of the charge and discharge characteristics of the 6.0 A-hr battery during T_C. This figure was obtained

---

[2] "Batteries for Space Power Systems," Paul Bauer, TRW Systems Group, Redondo Beach, California.

[3] The cyclic residual battery charge is the charge of the battery at any time during the orbit cycle.

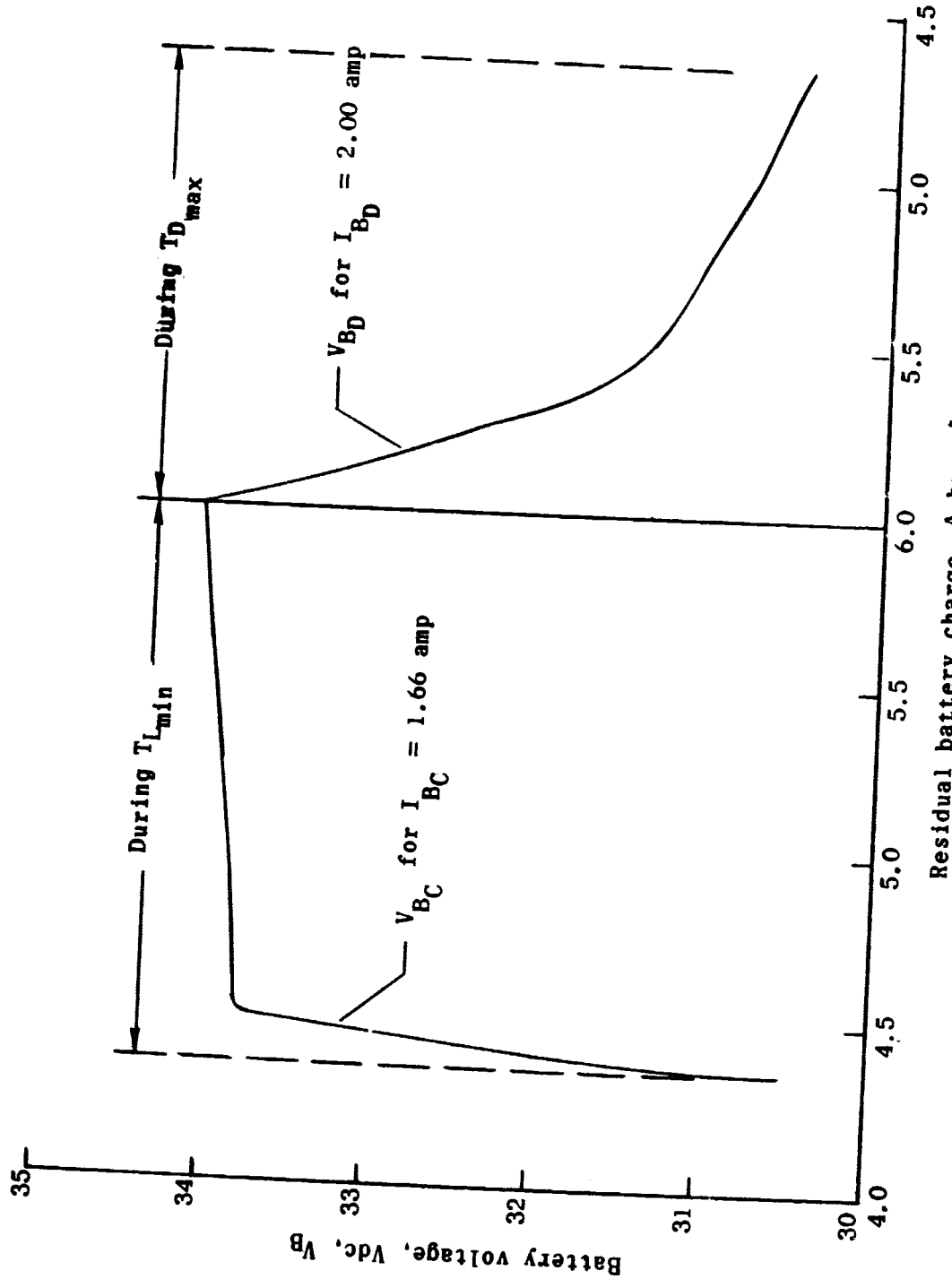

Figure 5.- Battery charge and discharge voltage vs. residual battery charge for constant-current battery-charge system.

by normalizing data of a Gulton Industries 12.0 A-hr Ni-Cd battery. This Gulton Industries battery was evaluated by the Spacecraft Power Systems Section (SPSS) of NASA, Langley Research Center. Although Figure 5 notes a constant I_{B_D} = 2.0 amp and a constant I_{B_K} = 1.66 amp, the figure is actually based on a Ni-Cd battery discharged at a constant rate of I_{B_D} = 1.75 amp and charged at a constant rate of I_{B_C} = 1.5 amp. This discrepancy was ignored in this analysis. According to Mr. Jim Bene, battery engineer of the Spacecraft Power System Section, the before mentioned discrepancy would not alter the results by more than 5 per cent.

Solar Array Size Determined

The size of the solar array is determined under conditions of $P_{L_{max}}$ and $T_{A_{max}}$ during T_C.

The required solar array terminal power (P_{IN}) is:

$$P_{IN} = \frac{P_L + (V_{B_C})(I_{B_K})}{EFF_R} \tag{7}$$

In Equation (7) during $T_{L_{min}}$; I_{B_K} = 1.66 amp and remains constant; V_{B_C} varies as shown in the charging portion of Figure 5; P_L can either be 56 w or 28 w but will be taken as 56 w in the array size determination, and EFF_R is described in Figure 4. During $T_{L_{min}}$, the input voltage to the regulator (V_R) is equal to the solar array terminal voltage (V_{IN}).

At $T_{A_{max}}$ = +110° C, the battery is fully charged, and V_{B_C} = 34.08 vdc. This can be seen with reference to Figures 1 and 5.

When $T_A = 110^\circ$ C, $T_L = 1$ hr as seen from Figure 1. Hence, at $T_A = 110^\circ$ C, 1.66 A-hr has been supplied to the battery since the beginning of the illuminated portion of the orbit. The addition of 1.66 A-hr to the residual battery charge (4.34 A-hr) at the beginning of the illuminated portion of the orbit gives 6.0 A-hr. With reference to Figure 5, a battery charge of 6.0 A-hr corresponds to a V_{B_C} of 34.08 vdc.

In Equation (7) substitute $P_L = 56$ w, $V_{B_C} = 34.08$ vdc, $I_{B_K} = 1.66$ A, and assume $EFF_R = 0.94$. This assumption will be made clearer at a later point in this section. When each of the values are substituted in Equation (7) $P_{IN} = 119.8$ w. The total number of solar cells (N_T) comprising the solar array is:

$$N_T = \frac{P_{IN}}{p_A} \tag{8}$$

where P_{IN} is the input required power at $T_A = 110^\circ$ C and p_A is the maximum available power per individual solar cell at $T_C = 110^\circ$ C. From Figure 2, $p_A = 16$ mw. Substituting $P_{IN} = 119.8$ w and $p_A = 16$ mw into Equation (8) $N_T = 7{,}480$. The number of series connected solar cells (N_S) per parallel string can be expressed as:

$$N_S = \frac{V_p}{v_p} \tag{9}$$

where V_p is the solar array terminal voltage at maximum power and v_p is the individual solar cell terminal voltage at maximum power.

From Figure 2, $v_p = 0.250$ vdc at $T_C = 110^\circ$ C. Let $V_p = 34.6$ vdc; substituting these values into Equation (9),

$$N_S = 139$$

The total number of parallel strings (N_p) of series connected solar cells is:

$$N_p = \frac{N_T}{N_S} \tag{10}$$

Substituting $N_T = 7{,}480$ and $N_S = 139$, we obtain

$$N_p = 54$$

The arbitrarily chosen value of $V_p = 34.6$ vdc results in a $EFF_R = 0.94$. Hence, the substitution of this EFF_R value in Equation (7) has been given a basis.

Figure 6 indicates the solar array characteristics of the CCS over the T_A range from -10° C to $+110^\circ$ C in 20° C intervals. Figure 6 shows the locus of solar array maximum available power (P_A) and the operating point loci for constant values of $P_{L_{max}}$ and $P_{L_{min}}$.

The solar array characteristic curves of Figure 6 were approximately drawn by calculating three points for each curve. By knowing three points and a general knowledge of the appearance of a solar array curve, each of the seven characteristic curves were drawn. The three points are obtained from Equations (11), (12), (13), and (14):

$$I_{sc} = N_P \, i_{sc} = 54 \, i_{sc} \tag{11}$$

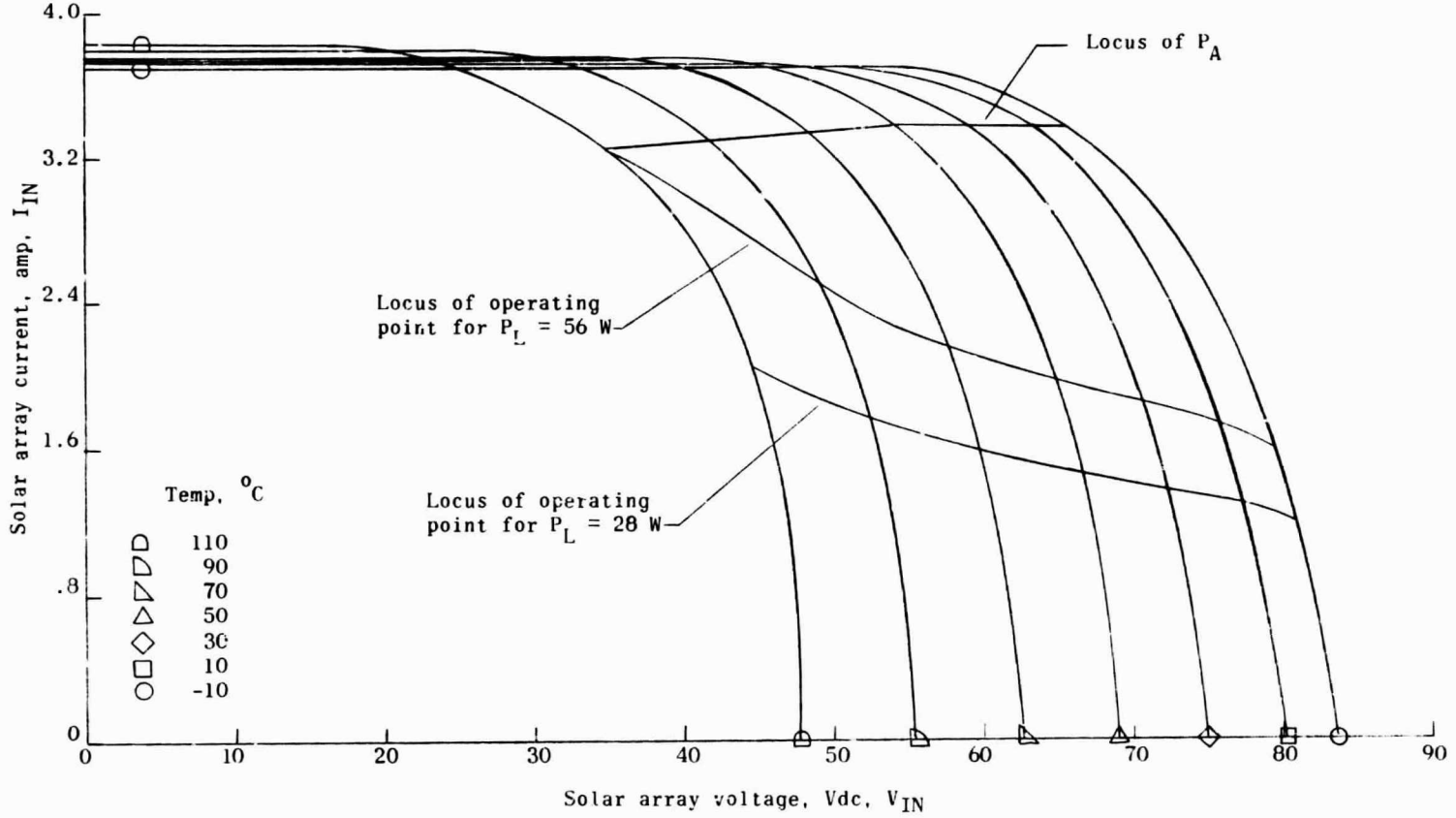

Figure 6.- Solar array characteristics for constant-current battery-charge system.

$$V_p = N_S v_p = 139 v_p \tag{12}$$

$$I_p = N_p i_p = 54 i_p \tag{13}$$

$$V_{OC} = N_S v_{oc} = 139 v_{oc} \tag{14}$$

Equation (11) results in the calculation of the short circuit load coordinate (the voltage coordinate is, of course, zero). Equation (12) and (13) gives the voltage and current coordinates of the maximum available power point. Equation (14) gives the voltage coordinate of the open load condition (the current coordinate is, of course, zero). The values of i_{sc}, v_p, i_p, and v_{oc} are obtained from Figure 2 for each of the seven T_A values shown in Figure 6. The faired-in curves of Figure 6 are sufficient to describe the CCS action.

The locus of maximum available power in Figure 6 is drawn by connecting points of maximum available power V_p, I_p for each of the seven T_A values indicated. The purpose of showing the P_A locus is to let it serve as a reference with relation to the two operating point loci, corresponding to $P_L = 56$ w and $P_L = 28$ w. Note how poorly the power capacity of the solar array is utilized in this figure. At only $T_A = +110^{\circ}$ C and $P_L = 56$ w is the solar array effectively utilized. At all other values of T_A for $P_L = 56$ w and for all values of T_A for $P_L = 28$ w, the solar array is ineffectively utilized. The reason for this ineffective use is that

for the CCS, the solar array can only be matched to its load at one value of T_A. For this analysis this value of T_A is 110° C. It will be shown that for the TCS, the solar array can be matched to its load over the full T_A range, as long as P_L remains at 56 w. For the TCS, if the value of P_L becomes 28 w, the solar array will be again mismatched to its load, however, the degree of mismatch will not be as severe as for the CCS for P_L = 28 w. The end result will be that the TCS will require a smaller solar array than the CCS.

The operating point loci of P_L = 56 w and P_L = 28 w in Figure 6 were obtained by working with Equation (7). In Equation (7), I_{B_K} remains constant at 1.66 amp and P_L is either 56 w or 28 w, depending on which of the two loci are being analyzed. The value of V_{B_C} is obtained by utilizing Figures 1 and 5. Figure 1 gives the corresponding value of T_L, with reference to the beginning of the illuminated portion of the orbit, for any value of T_A over its range. Multiplying this value of T_L by 1.66 amp gives the additional battery charge with reference to the beginning of the illuminated portion of the orbit. The sum of this additional battery charge plus the battery charge at the beginning of the illuminated portion of the orbit (4.34 A-hr) gives the residual battery charge at any time during T_L. Knowing this residual battery charge, V_{B_C} is obtained from Figure 5. Figure 7 indicates the variation of V_{B_C} versus T_A. The value of EFF_R in Equation (7) is obtained by an iterative method. The value of EFF_R depends on V_R, but during the illuminated interval, $V_R = V_{IN}$. The value of

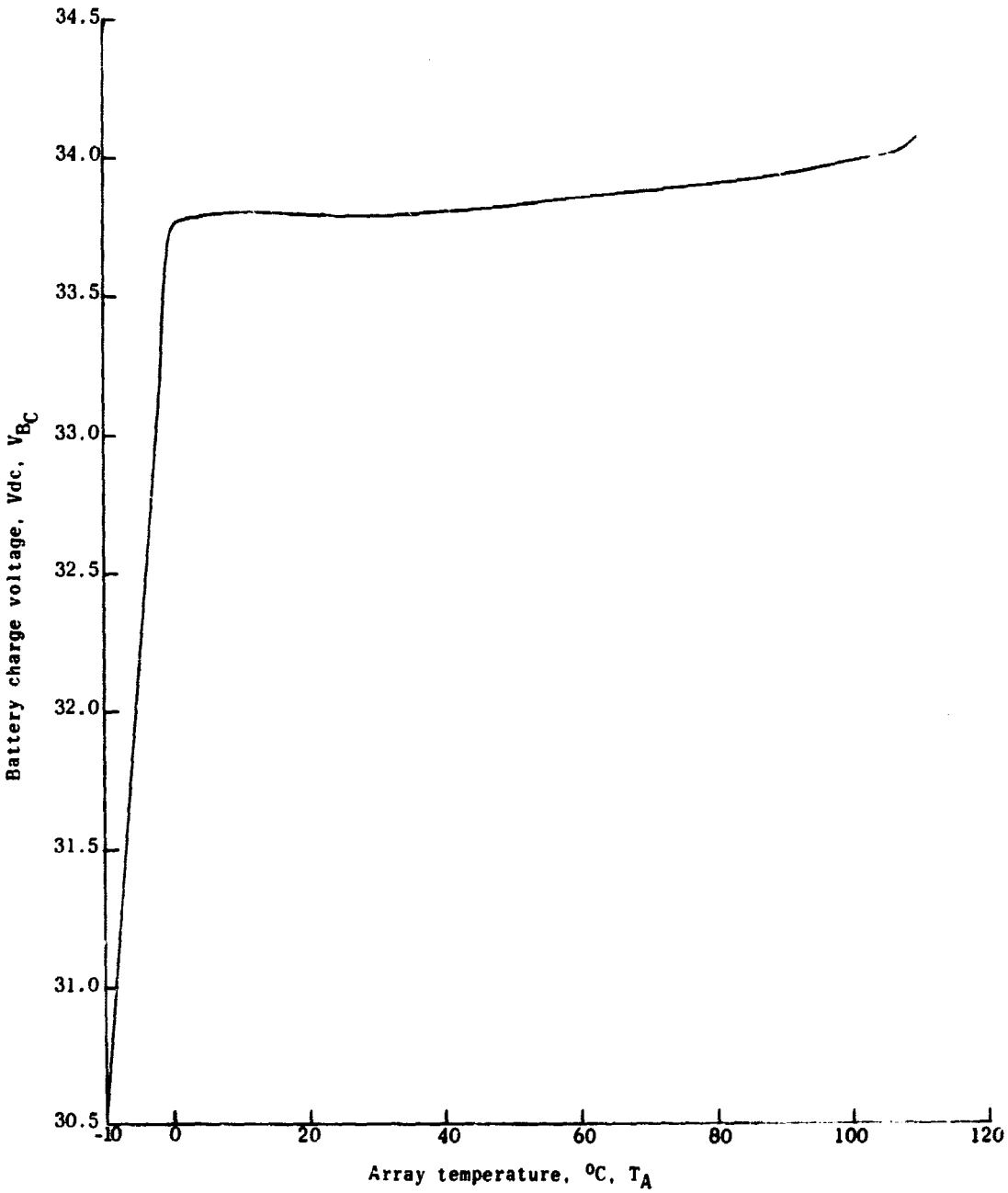

Figure 7.- Battery charge voltage vs. array temperature for constant current battery-charge system.

V_{IN} is dependent on the value of P_{IN} required, since $P_{IN} = (V_{IN})(I_{IN})$. This problem was attacked by assuming a value for EFF_R, and calculating P_{IN} using Equation (7). Next step was to find where the product of operating point voltage and operating point current equaled to the calculated P_{IN} value. When this operating point was found, the associated V_{IN} coordinate was used to find EFF_R from Figure 4. If the value of EFF_R was reasonably close to that assumed, then the set of values was self-consistent and the operating point was taken as valid. If the EFF_R value differed appreciably from the assumed value, then additional iterations of the above process were used to converge on the answer.

CHAPTER IV

TAPER-CURRENT BATTERY-CHARGE SYSTEM

The purpose of this chapter is to analyze the TCS, and show that its application leads to improved solar array utilization as compared to the CCS. The same Ni-Cd storage battery was utilized for both systems. Since the discharge energy requirements of both the CCS and TCS are identical, the discharge battery characteristic is represented as in Figure 5. The total amount of battery charge required is the same for both systems, however the method of charging the battery differs. The value of battery charging current, in the TCS, is continually adjusted such that the operating point of the solar array is matched to its load over the full T_A range as long as $P_{L_{max}}$ condition exists. As was the case for the CCS, the solar array size is determined under conditions of $P_{L_{max}}$ and $T_{A_{max}}$ during T_C.

Figure 8 represents the basic block diagram of the TCS. During T_L, the switch S_1 remains closed, and the solar array charges the battery and powers the experiments. During T_D, S remains open, and the battery discharges into the voltage regulator. The regulator output feeds the experiments. During T_L the solar array temperature sensor monitors T_A. The T_A sensor produces a signal proportional to T_A and feeds this signal into the taper charge control circuit (TCC). Also during T_L, the total experiment

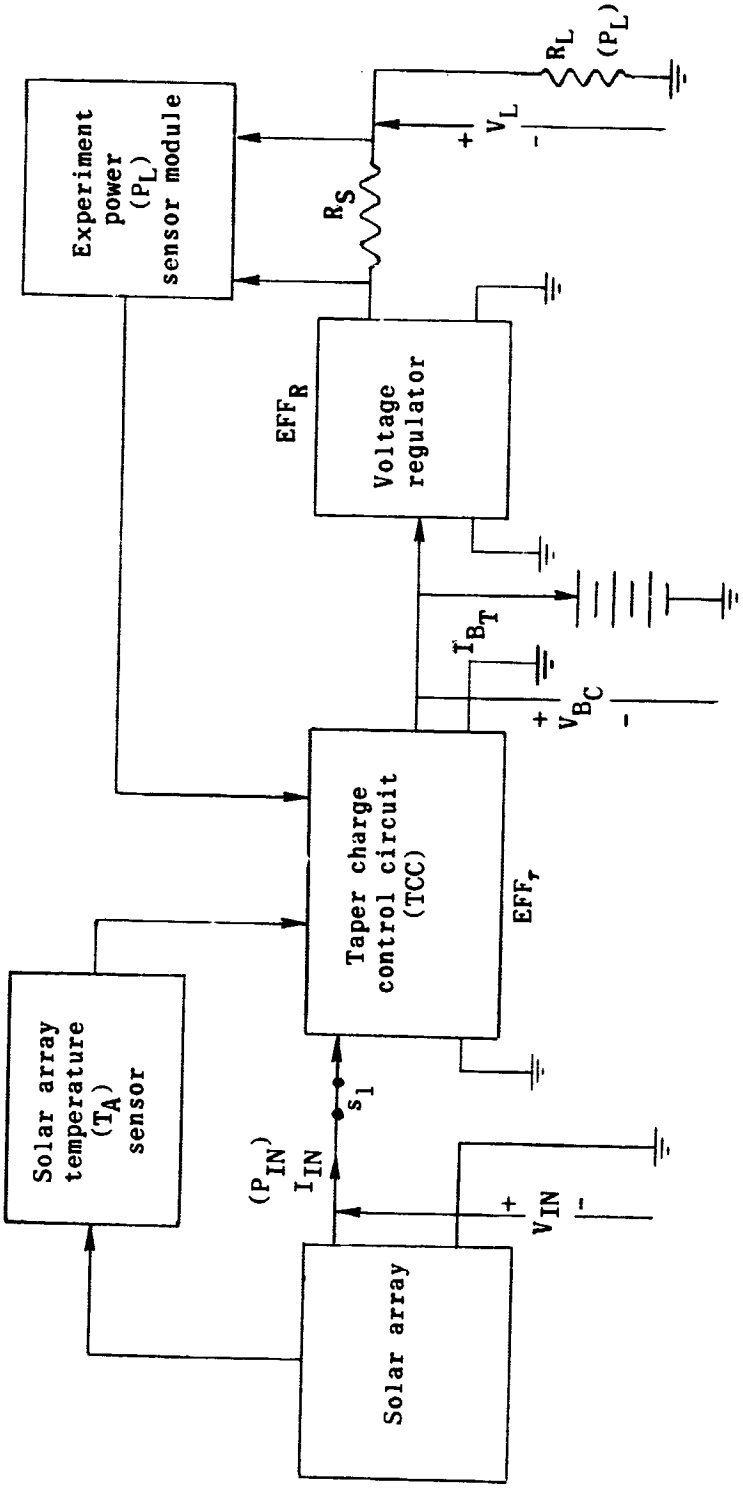

Figure 8.- Block diagram of taper-current battery-charge system.

power is sensed by a P_L sensor. The P_L sensor provides a signal that is either of two discrete values, depending whether $P_L = 56$ w or $P_L = 28$ w. Hence, the T_A sensor loop is analog in nature, whereas the P_L sensor loop is digital. The TCS operates such that as long as $P_L = 56$ w, the T_A sensor signal into the TCC forces the solar array to operate at its maximum power point over the T_A range of -10° C to $+110^{\circ}$ C. This action of controlling the solar array to operate at P_A is brought about by controlling the duty cycle (τ) of the TCC. Appendix I shows that:

$$\tau = \frac{V_{B_C}}{V_{IN}} \times 100 \tag{15}$$

The definitions for V_{B_C} and V_{IN} are the same as those given for the CCS and is shown in Figure 8 with relation to the TCS.

The TCC is essentially an electronic switch with associated logic circuitry. τ can also be defined as:

$$\tau = \frac{T_{ON}}{T_S} \times 100 \tag{16}$$

where T_S is the switching period of the electronic switch in the TCC, and T_{ON} is the on time of the electronic switch during T_S. Both Equations (15) and (16) are valid, but equation (15) is more useful in such an analysis as is being discussed. It will be shown in a later section of this thesis that the τ versus T_A function is continuous for either a constant value of $P_L = 56$ w or $P_L = 28$ w.

However, for a change in P_L from 56 w to 28 w or vice versa, a step function is introduced in the τ versus T_A function. In other words an abrupt shift in the τ versus T_A function occurs whenever P_L changes from one level to the other. As can be seen from Figure 8, the level of P_L is monitored by sensing I_L through a very low valued resistor.

There are various types of T_A sensors that could be utilized in the TCS, such as a thermistor, thermocouple, or even a solar cell. The latter two sensors have the advantage of generating a signal without need of a separate power supply or battery. The thermistor would probably require a bridge type arrangement. Such parameters as dynamic temperature range, measuring accuracy, and speed of thermal response would have to be considered in choosing a T_A sensor. The P_L sensor module perhaps could be a solid state inverter, whose output is always one of two states. The TCC perhaps could be an electronic switch, whose τ value is directly controlled by a saturable reactor or magnetic amplifier arrangement. For such an arrangement, the output signal from the P_L sensor could establish one of two quiescent bias levels for the magnetic amplifier, whereas the T_A sensor output signal would serve as the continually varying signal about either of the two quiescent levels. A general arrangement of a TCS, as previously discussed, will be described in somewhat greater detail at a later point in this thesis.

Battery Taper-Charge Current Philosophy

The proper battery taper-charge current $\left(I_{B_T}\right)$ versus T_A function will be of the general form of the maximum available power curve of Figure 2. In order to find the actual I_{B_T} versus T_A function that will fit in with the TCS philosophy, an interative process was employed: a linear I_{B_T} versus illuminated time function was assumed as a first trial (trial I). The solar array was sized-up, and the actual I_{B_T} versus illumination time function was found on the basis of trial I. A planimeter was used to find the total battery charge that accrued due to the actual I_{B_T} versus illumination time function of trial I. The difference between the required battery charge (1.66 A-hr) and the actual battery charge was used as a correction factor in trial II of the I_{B_T} solution. In working with this iterative process, the corresponding battery charge voltage $\left(V_{B_C}\right)$ versus illuminated time function was approximately found by a method of graphical interpolation based on the assumed linear I_{B_T}. Mr. Jim Bene, battery engineer at Spacecraft Power System Section, furnished curves of V_{B_C} versus time for four values of constant I_{B_C}. Since in the TCS, I_{B_C} is continually varying, it was necessary to interpolate between the curves of constant I_{B_C} in order to arrive at a representative V_{B_C} versus illuminated time function. The V_{B_C} versus illuminated time curve found from using interpolation has admittedly limited accuracy and only serves to provide information on the general character of the curve. Since this is

true, the V_{B_C} versus illuminated time curve found from trial I was assumed to hold for trial II even though the I_{B_T} curves for the two trials differ.

Battery Taper Charge Current - Trial I

Assume the I_{B_T} versus T_L function is of the linear nature shown in Figure 9. The maximum value of battery charging current $\left(I_{B_{T_{max}}}\right)$ occurs at $T_L = 0$, which corresponds to $T_A = -10^{\circ}$ C as seen from Figure 1. The minimum value of battery charging current $\left(I_{B_{T_{min}}}\right)$ occurs at $T_L = 1$ hr, which corresponds to $T_A = 110^{\circ}$ C. Let $T_L = 1$ hr be denoted by T_L', and so from Figure 9 we can write:

$$\xi_{B_T} = \left(I_{B_{T_{min}}}\right)\left(T_L'\right) + \frac{1}{2}\left(I_{B_{T_{max}}} - I_{B_{T_{min}}}\right)\left(T_L'\right) \qquad (17)$$

Substituting $T_L' = 1$ hr and $\xi_{B_T} = 1.66$ A-hr and simplifying we get:

$$I_{B_{T_{min}}} + I_{B_{T_{max}}} = 3.32 \qquad (18)$$

In order to determine the size of the solar array we must find the value of $I_{B_{T_{min}}}$. This is done by generating another equation involving $I_{B_{T_{min}}}$ and $I_{B_{T_{max}}}$. This second equation was obtained by working with Equation (19), which is based on Figure 8.

$$P_{IN} = p_A N_T = \frac{\frac{P_L}{EFF_R} + \left(V_{B_C}\right)\left(I_{B_T}\right)}{EFF_T} \qquad (19)$$

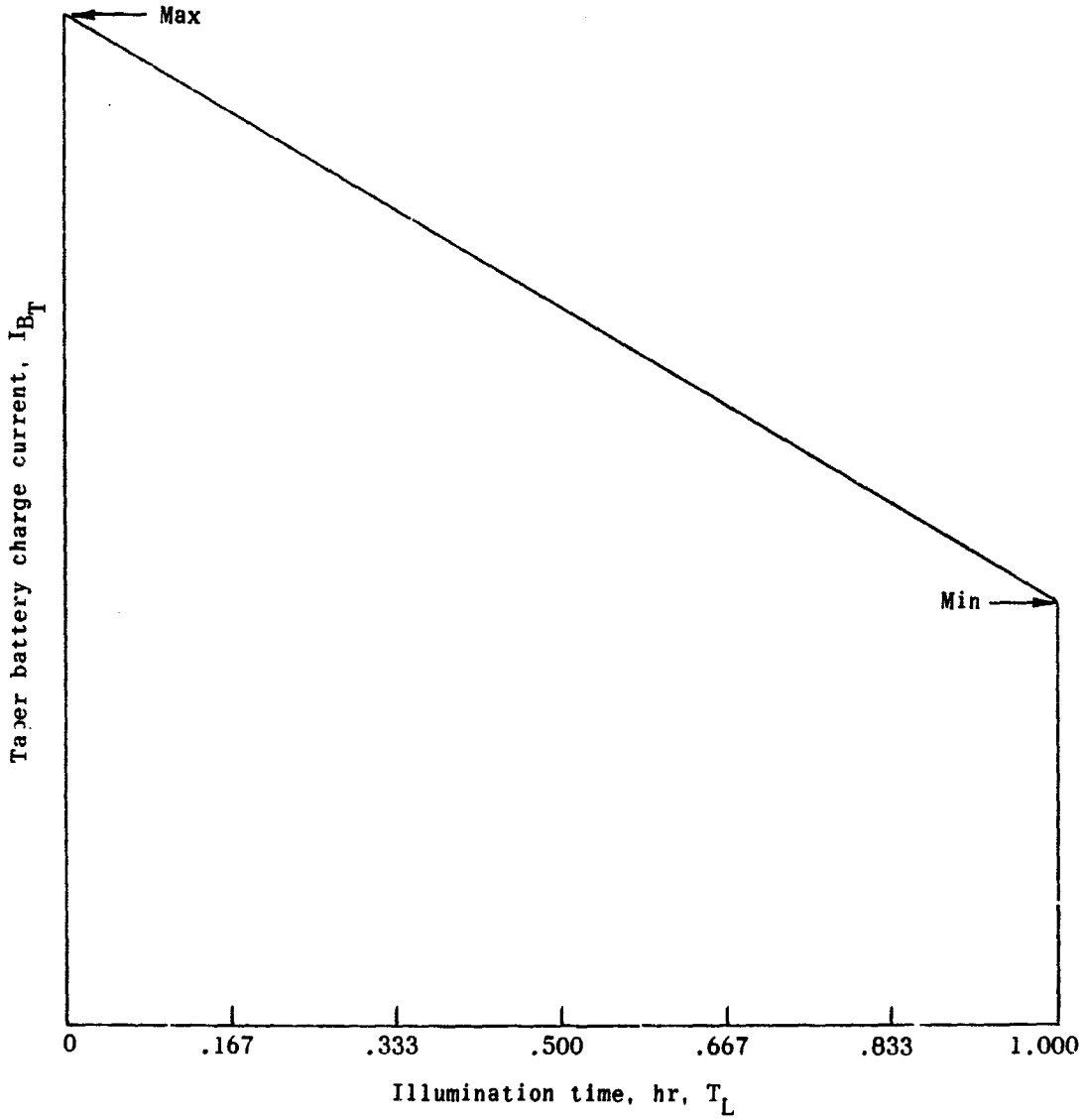

Figure 9.- Assumed contour of taper battery-charge current vs. illumination interval.

where:

P_{IN} is the required solar array terminal power, p_A is the maximum available solar cell power (obtained from Figure 2),

N_T is the total number of solar cells comprising the solar array,

P_L is the experiment power demand,

V_{B_C} is the battery charge voltage,

I_{B_C} is the battery charge current,

EFF_R is the efficiency of the voltage regulator (obtained from Figure 10), and

EFF_T is the efficiency of the TCC (obtained from Figure 11).

The EFF_R versus input regulator voltage of Figure 10 was arbitrarily assumed although the range of efficiency values are representative of nondissipative regulators. At $T_A = -10^{\circ}$ C, $p_A = 29.5$ mw, $V_{B_C} = 30.528$ vdc, $I_{B_C} = I_{B_{T_{max}}}$, $EFF_R = 0.90$, $EFF_T = 0.88$, and $P_L = 56$ w; substituting these values into Equation (19) and simplifying we obtain:

$$(29.5 \times 10^{-3}\ \text{w})\ N_T = 70.8 + 34.6\ I_{B_{T_{max}}} \qquad (20)$$

at $T_A = 110^{\circ}$ C, $p_A = 16$ mw, $V_{B_C} = 34.08$ vdc, $I_{B_C} = I_{B_{T_{min}}}$, $EFF_R = 0.85$, $EFF_T = 0.97$, and $P_L = 56$ w; substituting these values into Equation (19) and simplifying we obtain:

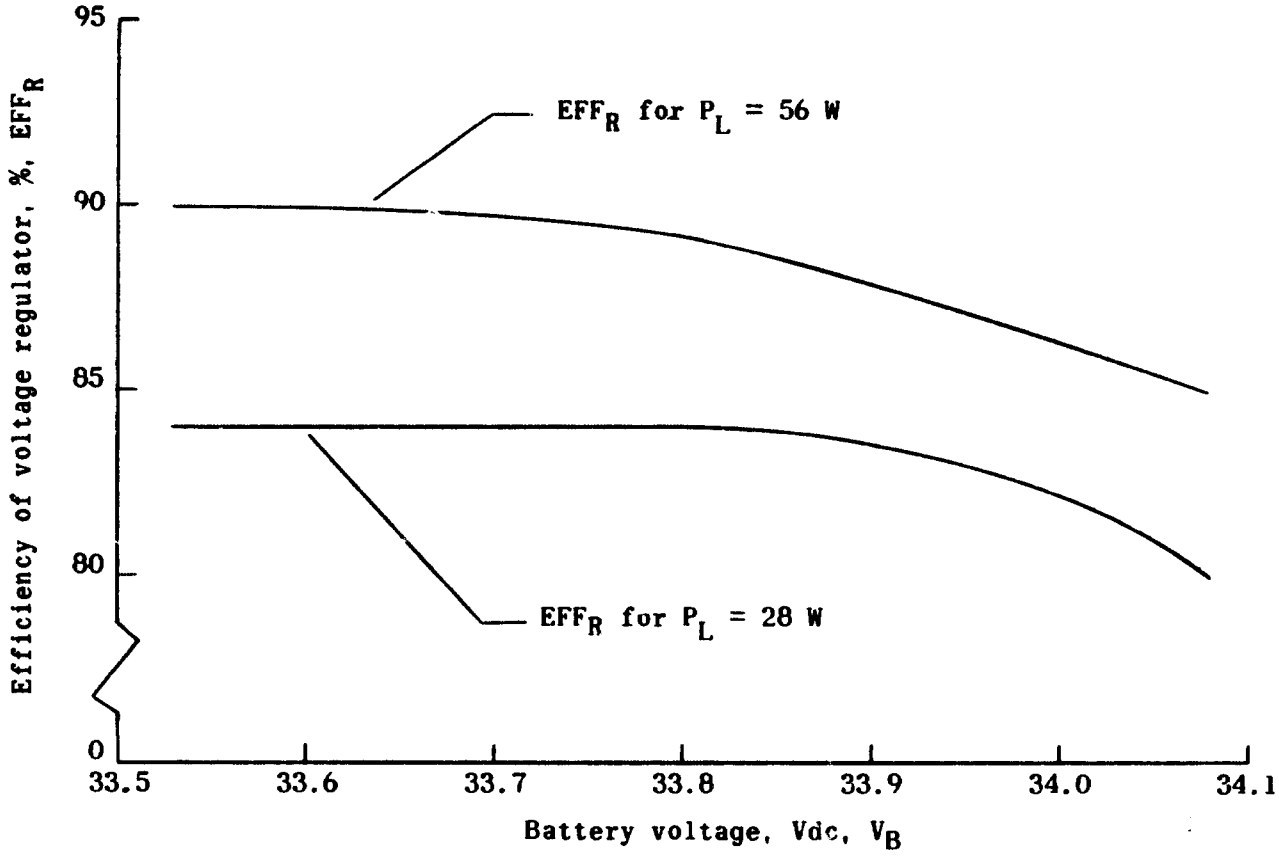

Figure 10.- Efficiency of voltage regulator vs. battery voltage for taper-current battery-charge system.

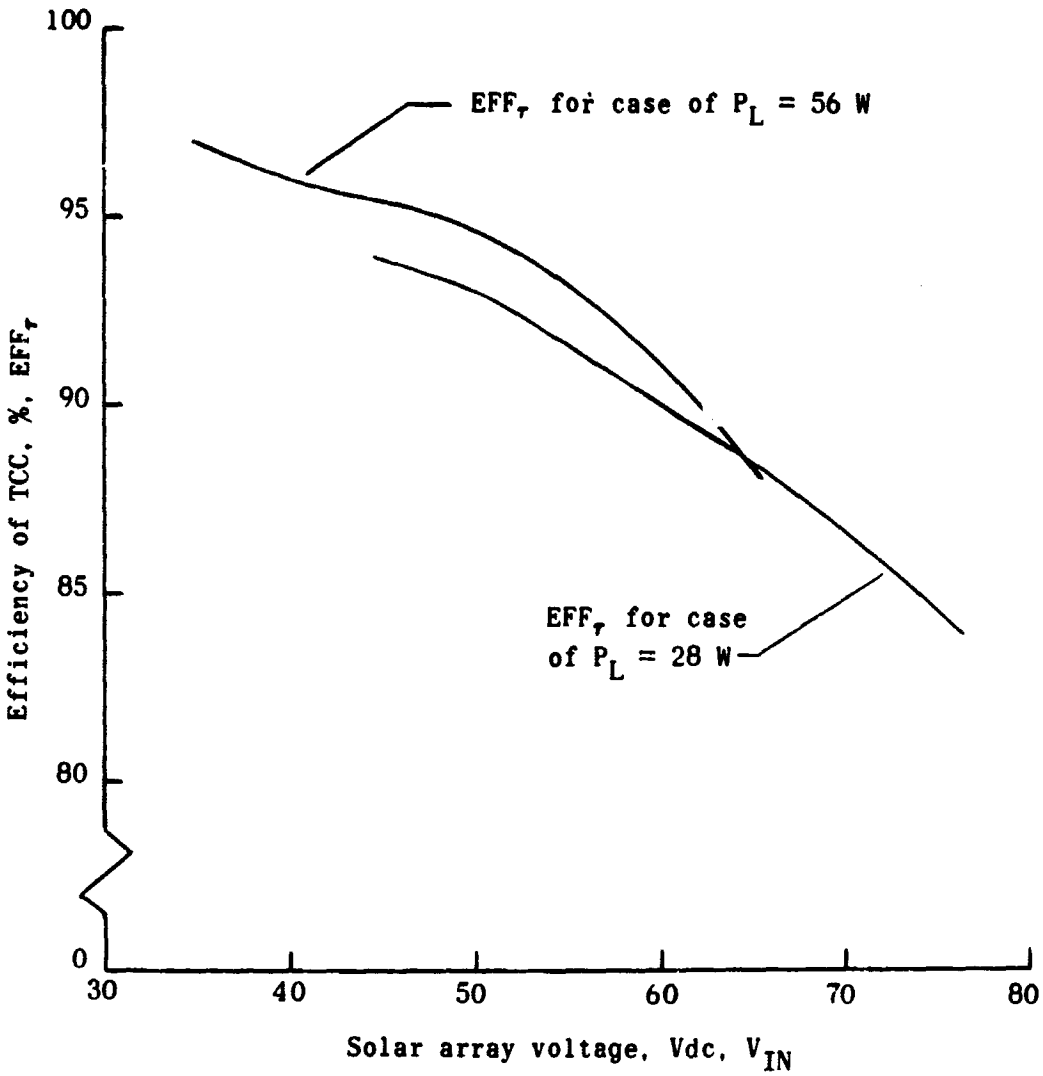

Figure 11.- Efficiency of taper control circuit vs. solar array voltage.

$$(16.0 \times 10^{-3}\ w)\ N_T = 67.8 + 35.2\ I_{B_{T_{min}}} \qquad (21)$$

The values of $EFF_T = 0.88$ and $EFF_T = 0.97$ in Equations (20) and (21), respectively, will be discussed at a later point in this analysis. Dividing Equation (21) into Equation (20) and simplifying, we obtain:

$$1.56 = I_{B_{T_{max}}} - 1.87\ I_{B_{T_{min}}} \qquad (22)$$

Solving Equations (18) and (22) simultaneously, we find that:

$$I_{B_{T_{min}}} = 0.612 \text{ amp}$$

$$I_{B_{T_{max}}} = 2.71 \text{ amp}$$

Sizing Up the Solar Array - Trail I

Knowing the value of I_{B_C} at $T_A = 110^\circ$ C, which is $I_{B_{T_{min}}}$, we are now in a position to determine the size of the solar array as a first trial. From Equation (19) and at $T_A = 110^\circ$ C, we see that:

$$N_T = \frac{\frac{P_L}{EFF_R} + \left(V_{B_C}\right)\left(I_{B_{T_{min}}}\right)}{\left(p_A\right)\left(EFF_T\right)} \qquad (23)$$

Substituting: $P_L = 56$ w, $EFF_R = 0.85$, $V_{B_C} = 34.08$ vdc, $I_{B_{T_{min}}} = 0.612$ amp, $p_A = 16 \times 10^{-3}$ w, and $EFF_T = 0.97$, we obtain:

$$N_T = 5{,}580 \text{ solar cells}$$

Rewriting Equation (9):

$$N_S = \frac{V_P}{v_p} \tag{9}$$

In Equation (9) $v_p = 0.25$ vdc as seen from Figure 2. The question of V_P can be answered from a consideration of τ. Let $\tau = 100$ per cent at $T_A = 110^\circ$ C. From Equation (15), since $V_{B_C} = 34.08$ vdc, this implies $V_{IN} = 34.08$ vdc. However, as is discussed in Appendix I, there is always a small voltage drop across the main power elements in the TCC. In order to compensate for this fact let $V_{IN} = 34.6$ vdc. Hence, substituting in the values: $v_p = 0.250$ vdc and $V_{IN} = V_P = 34.6$ vdc, we obtain from Equation (9) that:

$$N_S = 139$$

Rewriting Equation (10)

$$N_P = \frac{N_T}{N_S} \tag{10}$$

Substituting the values of $N_T = 5{,}580$ and $N_S = 139$, we obtain

$$N_P = 40$$

The chosen value of $EFF_\tau = 0.97$ in Equation (19) for $T_A = 110^\circ$ C has been given a basis, since from Figure 11 and $V_{IN} = 34.6$ vdc, the value of EFF_τ is 0.97.

The next step in the analysis is to see if the determined solar array size is sufficient to fully charge the battery during $T_{L_{min}}$. This can be studied by working with Equation (24)

$$I_{B_T} = \frac{P_A \left(EFF_T\right) - \frac{P_L}{EFF_R}}{V_{B_C}} \tag{24}$$

In Equation (24) P_A is the maximum available power at the solar array terminals at any chosen T_A.

The following procedure was used with Equation (24) to obtain the I_{B_C} versus T_L curve and hence, ξ_{B_T} data. First I_{B_C} versus T_A information was generated. In order to do this, information of each of the terms on the right side of Equation (24) versus T_A must be obtained.

P_A versus T_A information is easily obtained since

$$P_A = N_T\, p_A = 5{,}580\, p_A \tag{25}$$

By choosing values of T_A over the range of -10° C to 110° C and obtaining p_A from Figure 2, P_A versus T_A was defined.

The value of EFF_T depends on the solar array terminal voltage $\left(V_{IN}\right)$, as noted in Figure 11. However, for the case of $P_L = 56$ w, $V_{IN} = V_P$. From Equation (26)

$$V_P = N_S\, v_p = 139\, v_p \tag{26}$$

we see that V_P versus T_A is defined since v_p is obtainable from Figure 2. Hence, EFF_T versus T_A is defined.

P_L is taken as 56 w since we have to size the solar array under the $P_{L_{max}}$ condition.

It takes some work to find V_{B_C} versus T_A. Once V_{B_C} versus T_A is known, EFF_R versus T_A is also known, since EFF_R is defined in terms of V_{B_C} in Figure 10. Figure 12 shows the four constant current battery charging curves (obtained from Mr. Jim Bene, battery engineer at Spacecraft Power System Section) and the resulting interpolated curve. The interpolated curve is based on the linear I_{B_T} shown in Figure 9 with the calculated values of $I_{B_{T_{max}}}$ and $I_{B_{T_{min}}}$ of 2.71 amp and 0.612 amp, respectively. From the interpolated curve of Figure 12 and Figure 1, V_{B_C} versus T_A is obtained and shown in Figure 13.

Taking the information from Equation (25) and Figures 10, 11, and 13, and inserting this data in Equation (24), we define I_{B_C} versus T_A. From the I_{B_C} versus T_A information and Figure 1, I_{B_C} versus T_L is obtained. The resulting I_{B_C} versus T_L curve is shown in Figure 14. With the use of a planimeter, the ξ_B associated with this curve was found to be 1.43 A-hr. Hence, for trial I, the size of the solar array is insufficient, since an ξ_{B_T} of 1.66 amp-hr was required. A second trail is necessary.

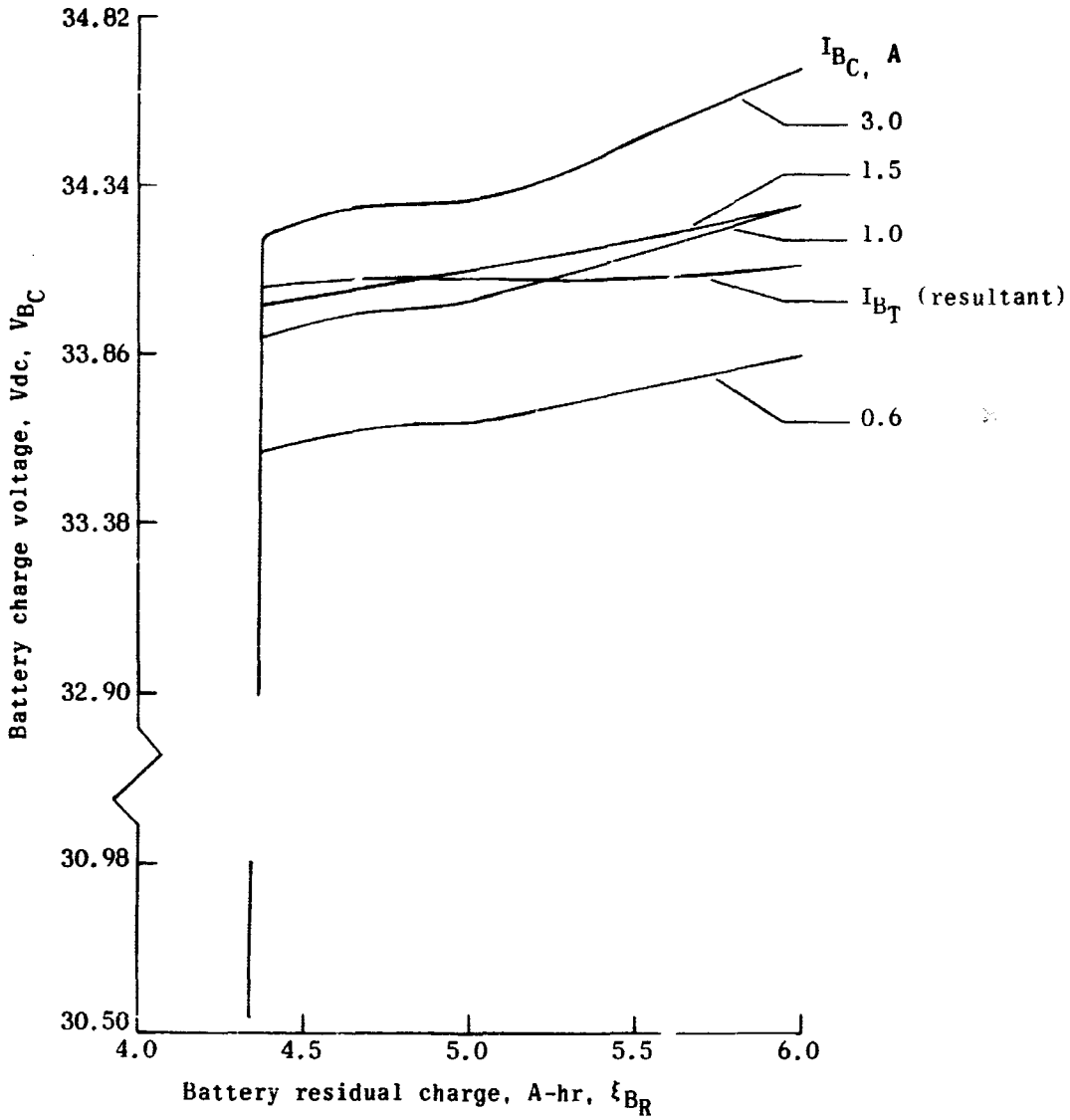

Figure 12.- Battery charge voltage vs. residual battery-charge for taper-current battery-charge system.

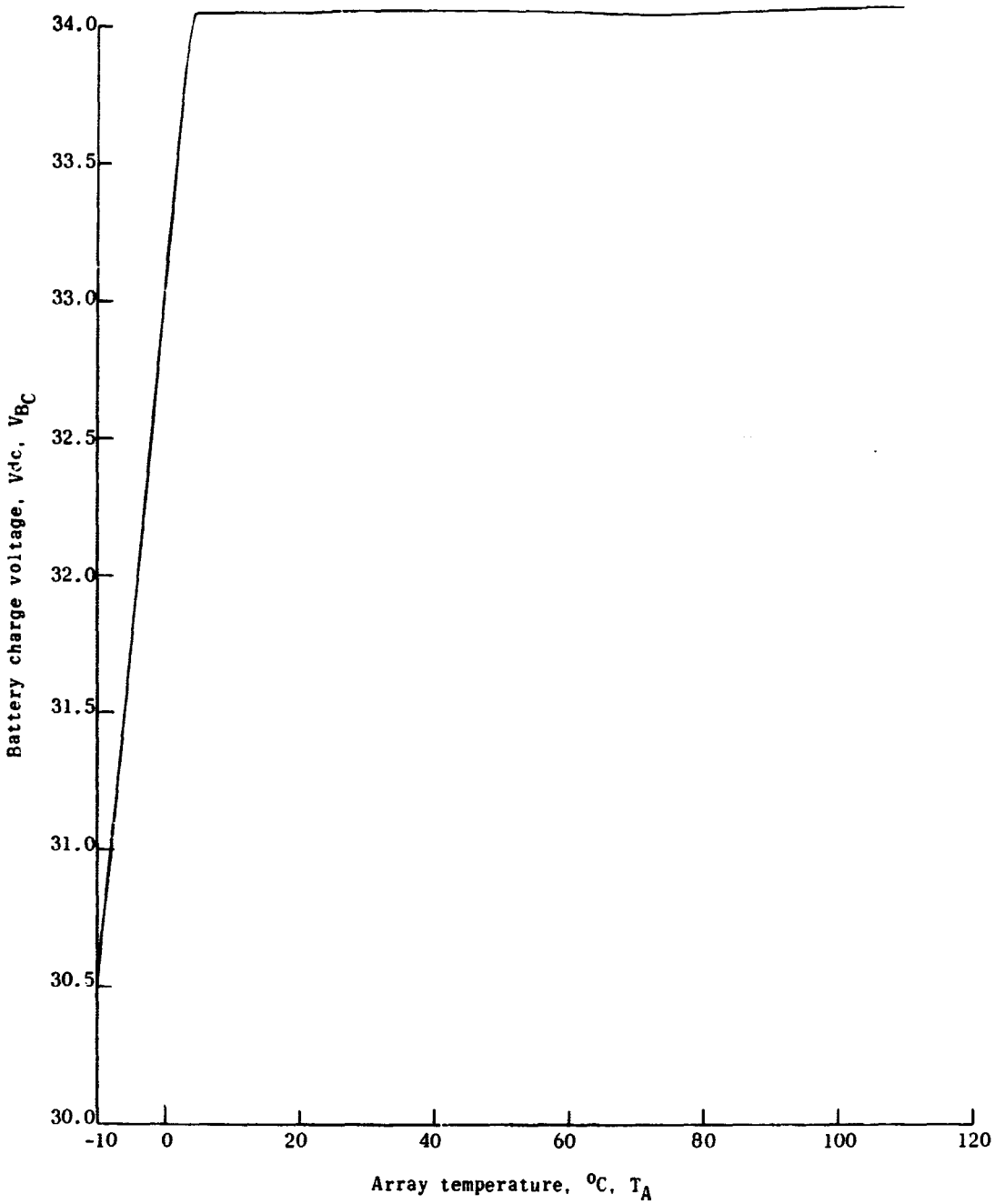

Figure 13.- Battery charge voltage vs. array temperature for taper-current battery-charge system.

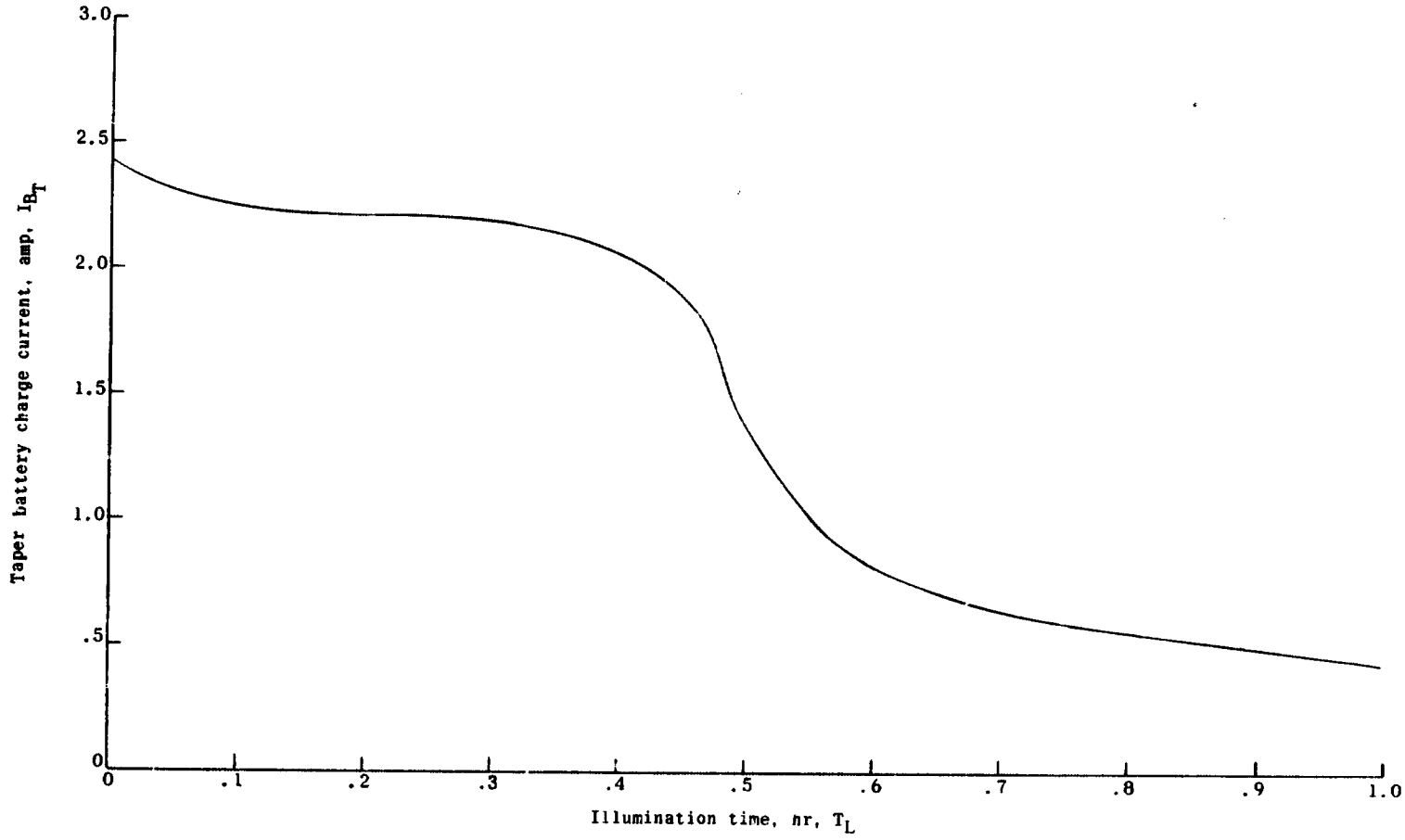

Figure 14.- Battery taper charge current resulting from trial I.

Battery Taper Charge Current - Trial II

We require an ξ_{B_T} = 1.66 A-hr. From trial I, an ξ_{B_T} = 1.43 A-hr. was obtained. Trail I resulted in a deficiency of ξ_{B_T} of 0.23 A-hr. Let trial II again assume linear I_{B_T} versus T_L function as shown in Figure 9. However for Trial II insert a correction of 0.23 A-hr. In other words base the ξ_{B_T} on a value: 1.66 + 0.23 = 1.89 A-hr. This philosophy is employed since it is believed that again a nominal ξ_{B_T} deficiency of 0.23 A-hr will result, and hence, resulting in the desired ξ_{B_T} value.

For trial II it is necessary to solve for $I_{B_{T_{min}}}$. This can be done by solving Equations (17) and (22) simultaneously. Equation (17), for trial II, has the substituted values of ξ_{B_T} = 1.89 A-hr and T_L' = 1 hr. The simultaneous solution of Equations (17) and (22) results in values:

$$I_{B_{T_{max}}} = 3.0 \text{ amp}$$

$$I_{B_{T_{min}}} = 0.77 \text{ amp}$$

Sizing Up the Solar Array - Trial II

In order to determine the size of the solar array for trial II, the same procedure as employed in trial I is utilized. It is assumed that the V_{B_C} versus T_A curve for trial II is the same as for trial I and shown in Figure 13.

In order to determine the total number of solar cells comprising the solar array (N_T), Equation (23) is again utilized. For $T_A = 110^{\circ}$ C and substituting the same values into Equation (23) as for trial I, with the exception of $I_{B_{T_{min}}} = 0.77$ amp (instead of 0.612 amp), we obtain:

$$N_T = 5,950 \text{ solar cells}$$

In other words, based on trial II, the solar array size had to be increased from 5,580 to 5,950 solar cells. To find N_S, Equation (9) is used and since the values of V_P and v_p remain unchanged, then

$$N_S = 139$$

Using Equation (10) and substituting in the values of $N_T = 5,950$ and $N_S = 139$, we find

$$N_P = 43$$

In order to examine if trial II solar array results in enough ξ_{B_T}, Equation (24) again has be dealt with in the same fashion as described for trial I. Briefly reviewing the operation, we obtain I_{B_C} versus T_L by first generating I_{B_C} versus T_A information. In Equation (24) P_A versus T_A data can be obtained from

$$P_A = N_T p_A = 5,950 p_A \tag{27}$$

The EFF_T versus T_A data is generated from Figure 11 and Equation (26). P_L is considered to be 56 w and constant versus T_A. The

case of $P_L = 28$ w will be discussed in the next section. V_{B_C} versus T_A is shown in Figure 13, and EFF_R versus T_A is defined from Figures 10 and 13. After obtaining I_{B_C} versus T_A, Figure 1 is used to find I_{B_C} versus T_L. The resulting I_{B_C} versus T_L for trial II is shown in Figure 15. Using a planimeter to find the area bounded by Figure 14, we thereby find:

$$\xi_{B_T} = 1.79 \text{ A-hr}$$

Hence, the required battery charge is obtained from trial II.

Solar Array Characteristics for TCS

The solar array that satisfies the ξ_{B_T} requirement for the TCS consists of

$$N_T = 5,950$$

$$N_S = 139$$

$$N_P = 43$$

The characteristics of this solar array are shown in Figure 16. This figure shows the array characteristics versus T_A, over the T_A range of -10° C to 110° C in 20° C intervals. Also shown are the locus of maximum available power P_A and operating point loci for constant values of $P_L = 56$ w and $P_L = 28$ w.

The method of constructing the array characteristics is identical to that described in "Solar Array Size Determined" section

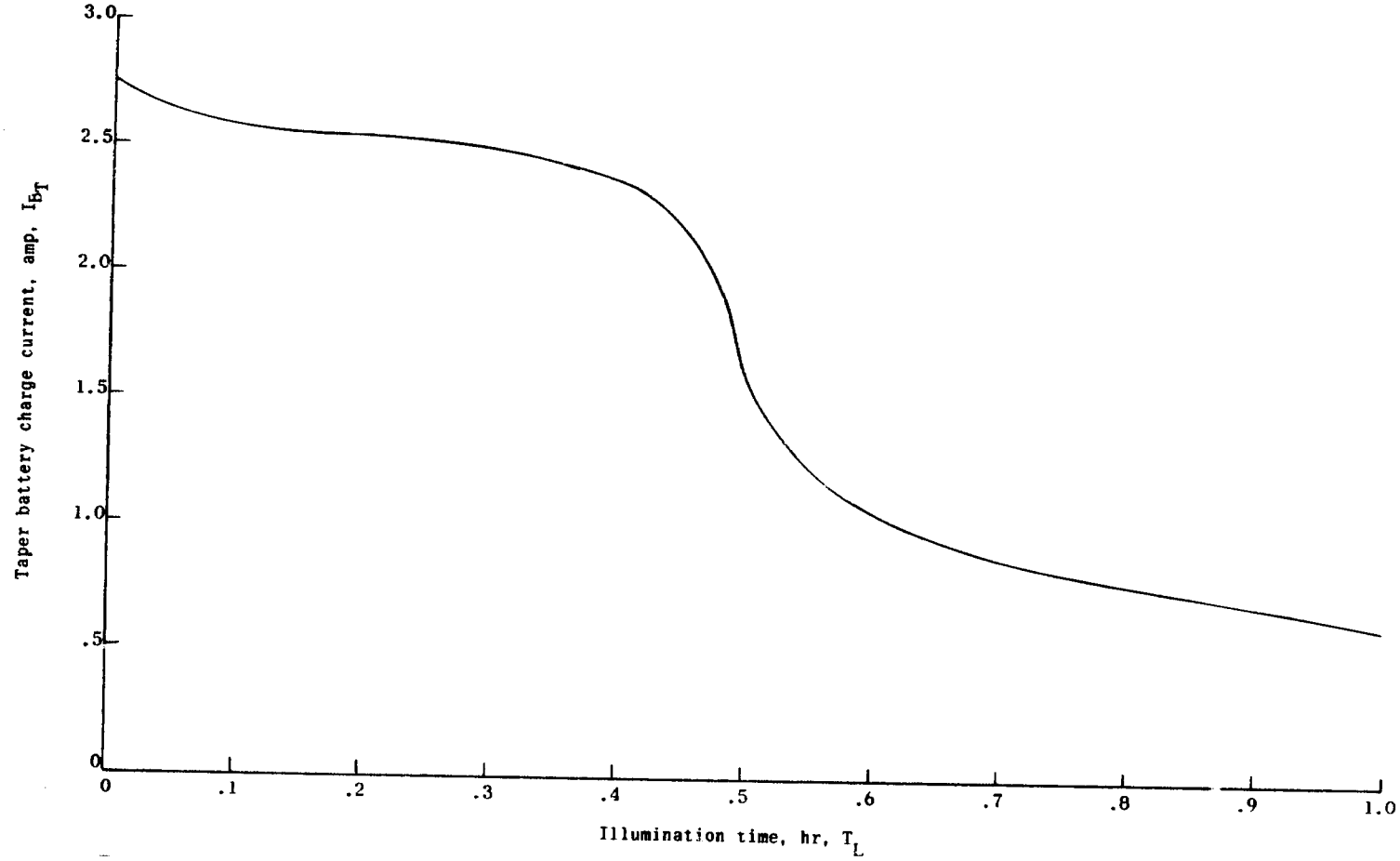

Figure 15.- Battery taper charge current resulting from trial II.

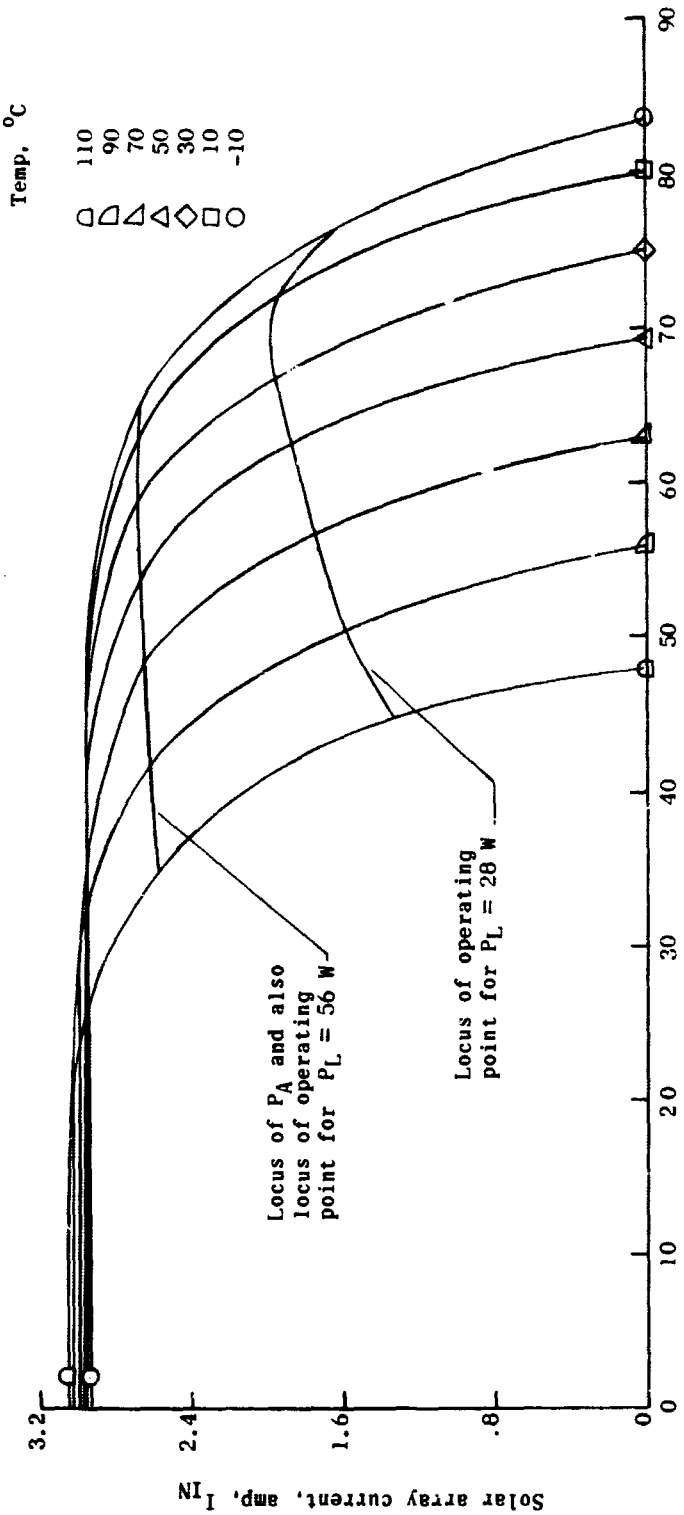

Figure 16.- Solar array characteristics for taper-current battery-charge system.

for the CCS. Each of the seven characteristic curves are based on the calculation of three points which must fall on the curve. These three points are obtained from:

$$I_{sc} = N_P \, i_{sc} = 43 \, i_{sc} \tag{28}$$

$$V_P = N_S \, v_p = 139 \, v_p \tag{29}$$

$$I_P = N_P \, i_p = 43 \, i_p \tag{30}$$

$$V_{OC} = N_S \, v_{oc} = 139 \, v_{oc} \tag{31}$$

The values of i_{sc}, v_p, i_p, and v_{oc} are obtained from Figure 2.

The locus of P_A is simply obtained by connecting the V_P, I_P coordinates of each characteristic curve.

The operating point loci for $P_L = 56$ w and $P_L = 28$ w were constructed by working with Equation (19). In Equation (19) P_L is either 56 w or 28 w, V_{B_C} is obtained from Figure 13, I_{B_C} is obtained from Equation (24), EFF_R is obtained from Figure 10, and EFF_T is obtained from Figure 11. For the case of $P_L = 56$ w, EFF_T is simply obtained from Figure 10, since $V_{IN} = V_P$. However, for the case of $P_L = 28$ w, the value of V_{IN}, which is one of the two coordinates defining the mismatched state, is not known. Since V_{IN} is unknown, EFF_T is unknown, and hence, P_{IN} is unknown. This problem was overcome by assuming a value of EFF_T and calculating P_{IN} from

Equation (19). After P_{IN} was calculated, a trial and error procedure was used to find the point on the characteristic curve of Figure 16, at the T_A of interest, where $(V_{IN})(I_{IN}) = P_{IN}$. After finding the coordinates of this point, the value of EFF_T was found from Figure 11 and compared against the assumed EFF_T value. If the assumed and obtained EFF_T values were reasonably close then the assumption was considered valid. If they differed appreciably, then another EFF_T value was assumed at the same T_A value under consideration and the process repeated, and so forth.

Note from Figure 16, the degree of utility of the solar array as compared to Figure 6. The key to the utility difference is that for Figure 16 (TCS) the array is forced to operate at P_A throughout the T_A range, whereas in Figure 6 (CCS) the array operates at P_A only at $T_A = 110^{\circ}$ C. The improvement in array utility is evident at both $P_L = 56$ w and at $P_L = 28$ w.

Figure 17 indicates the variation of τ versus T_A for constant values of $P_L = 56$ w and $P_L = 28$ w. For the case of $P_L = 56$ w, $\tau = \frac{V_{B_C}}{V_P}$. Whereas for the case of $P_L = 28$ w, $\tau = \frac{V_{B_C}}{V_{IN}}$; V_{IN} is the array terminal voltage coordinate of the mismatched condition. Also shown in Figure 17 is the effect on the τ curve of a change in P_L from 56 w to 28 w. This change in P_L was arbitrarily chosen to take place at $T_A = 50^{\circ}$ C.

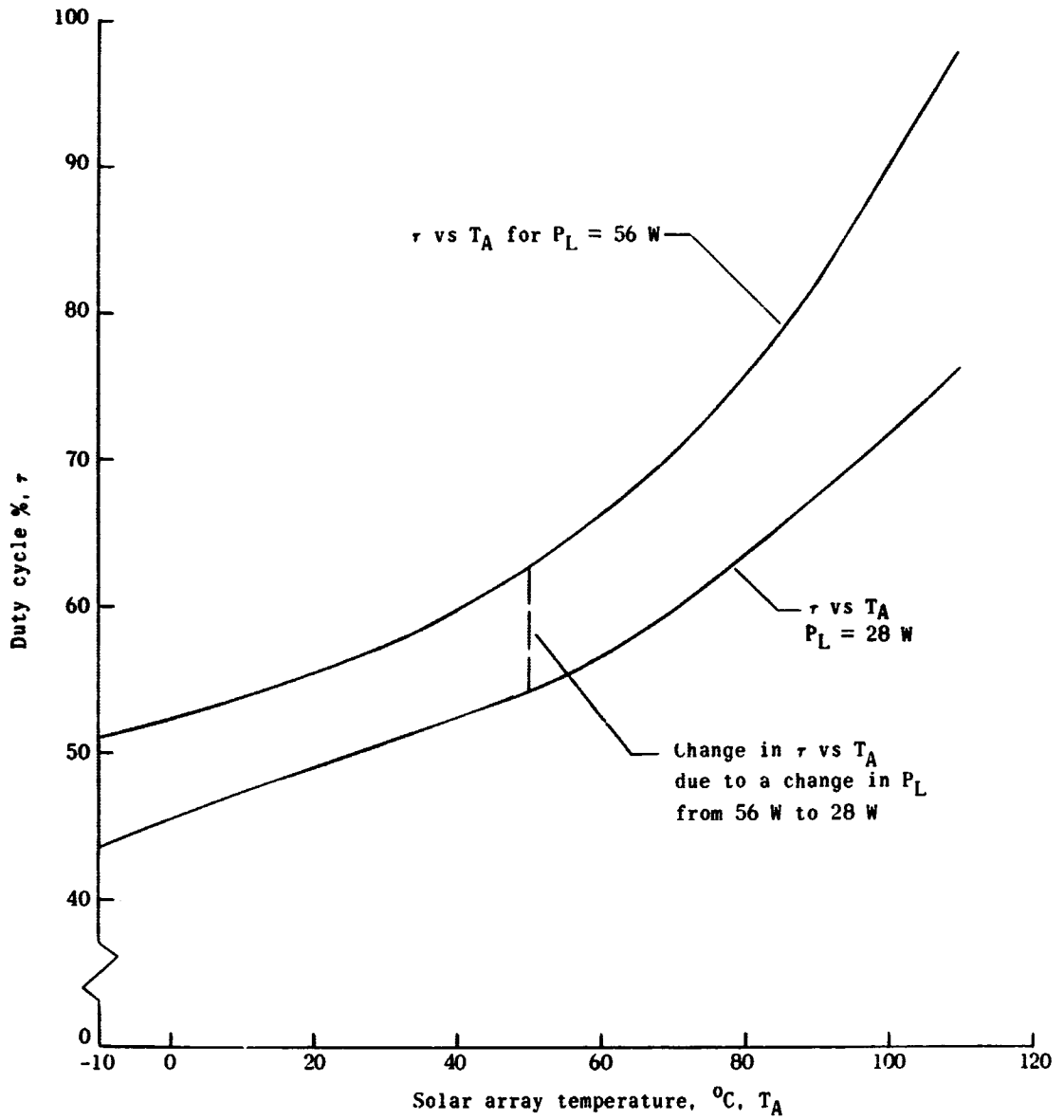

Figure 17.- Duty cycle vs. array temperature.

CHAPTER V

COMPARISON BETWEEN CCS AND TCS

It has been shown that the TCS is superior to the CCS on the basis of solar array utility. The purpose of this section is to compare the two systems on the basis of solar array area, weight, and cost. According to Mr. John L. Patterson, section head of Spacecraft Power System Section, the solar array area, weight, and cost can be described as*

$$A = \left(\frac{1\ ft^2}{10\ w}\right)\left(P_S\right)$$

That is, one square foot of solar array panel area generates 10 watts of electricity (this is based on an illumination intensity of approximately 140 $\frac{mw}{cm^2}$)

$$WT = \left(\frac{2\ lb}{ft^2}\right)(A)$$

$$C = \left(\frac{\$1,000.00}{w}\right)\left(P_S\right)$$

That is, the cost of a solar array is approximately $1,000 per watt operated. Where:

A is the cross sectional area of the solar array,

P_S is the power capacity of the array at the T_A for which the array's size was determined,

---

*These A, WT, and C rule of thumb figures include solar cells and their irradiation shields.

WT is the weight of the solar array, and

C is the cost of the solar array.

For the CCS

$$A = \left(\frac{1\ ft^2}{10\ w}\right)(119.8\ w) = 11.98\ ft^2$$

$$WT = \left(\frac{2\ lb}{ft^2}\right)(11.98\ ft^2) = 23.96\ lb$$

$$C = \left(\frac{\$1,000.00}{w}\right)(119.8\ w) = \$119,800.00$$

For the TCS

$$A = \left(\frac{1\ ft^2}{10\ w}\right)(95.3\ w) = 9.53\ ft^2$$

$$WT = \left(\frac{2\ lb}{ft^2}\right)(9.53\ ft^2) = 19.06\ lb$$

$$C = \left(\frac{\$1,000.00}{w}\right)(95.3\ w) = \$95,300.00$$

As can be seen from the results the TCS gives improvement in solar array area, weight, and cost.

In the preceding comparison only the required solar array of each system was compared. A somewhat more meaningful comparison would result if the power conditioning of the two systems were also compared. Observing the block diagrams of the two systems, shown in Figures 3 and 8, it is seen that more subassemblies are required for the TCS. The difference lies in the fact that the TCS requires a TCC,

a T_A sensor, a P_L sensor, and P_L sensor module. Since the power handling requirements of these preceding mentioned subassemblies are very small, their respective area, weights, and power source requirements should be very small. Furthermore the area, weight, and power source requirements of these mentioned subassemblies are independent of the nominal power capacity requirement of the solar array. Hence, relative advantages of the TCS over the CCS increase as the power capacity requirement of the array increase. For the chosen nominal array power capacity in this thesis, the relative advantages in A, WT, and C of the TCS are not as good as depicted from the calculations in this section, due to the extra subassemblies of the TCS. However, the TCS is still superior, even for a nominal array power of 100 w, since these subassemblies do not tax A, WT, and C to a substantial degree.

A word of caution should be stated in the comparison of the TCS with the CCS. The actual resultant design advantage obtainable by utilizing the principles of taper battery charging is somewhat affected by the temperature history actually experienced by the solar array. In the extreme situation where the solar array operates at maximum array temperature throughout the illumination interval, the two designs (TCS and CCS) use the same number of solar cells. Hence, for this case, there is no relative advantage of the TCS over the CCS. The area between the actual array temperature curve and highest temperature level (as shown in Fig. 1) is an indicator of attainability for the nominal 25 per cent relative advantage described in this comparative analysis.

CHAPTER VI

TAPER CURRENT BATTERY CHARGE SYSTEM CANDIDATE

A general candidate for the TCS is shown in Figure 18. The main areas of interest in this figure are the saturable core reactor, the T_A sensor, and the P_L sensor module.

The heart of the taper charge control circuit (TCC) in Figure 18 is the saturable core reactor. A square wave oscillator, such as a transistorized magnetic multivibrator, feeds low level power to the saturable core reactor through windings, N_6 and N_7. The oscillator is designed to operate at a constant repetition frequency. One pair of windings $(N_1$ and $N_2)$ drives the switching power transistors $(Q_{S_1}$ and $Q_{S_2})$. Q_{S_1} and Q_{S_2} interrupt the main power, which is supplied by the solar array, and ultimately is utilized to charge the battery and power the experiments. The switching frequency of Q_{S_1} and Q_{S_2} remains constant and is equal to the frequency of the square wave oscillator. By varying the symmetry of the square wave drive at the bases of Q_{S_1} and Q_{S_2}, the duty cycle (τ) is varied. In order to vary the drive symmetry, it is necessary to vary the magnetic operating point of the saturable core reactor.

The magnetic operating point of the saturable core reactor is varied in a continuous manner by the output signal of the solar array temperator T_A sensor. A good choice for the T_A sensor would be an individual solar cell. This T_A measuring solar cell could be

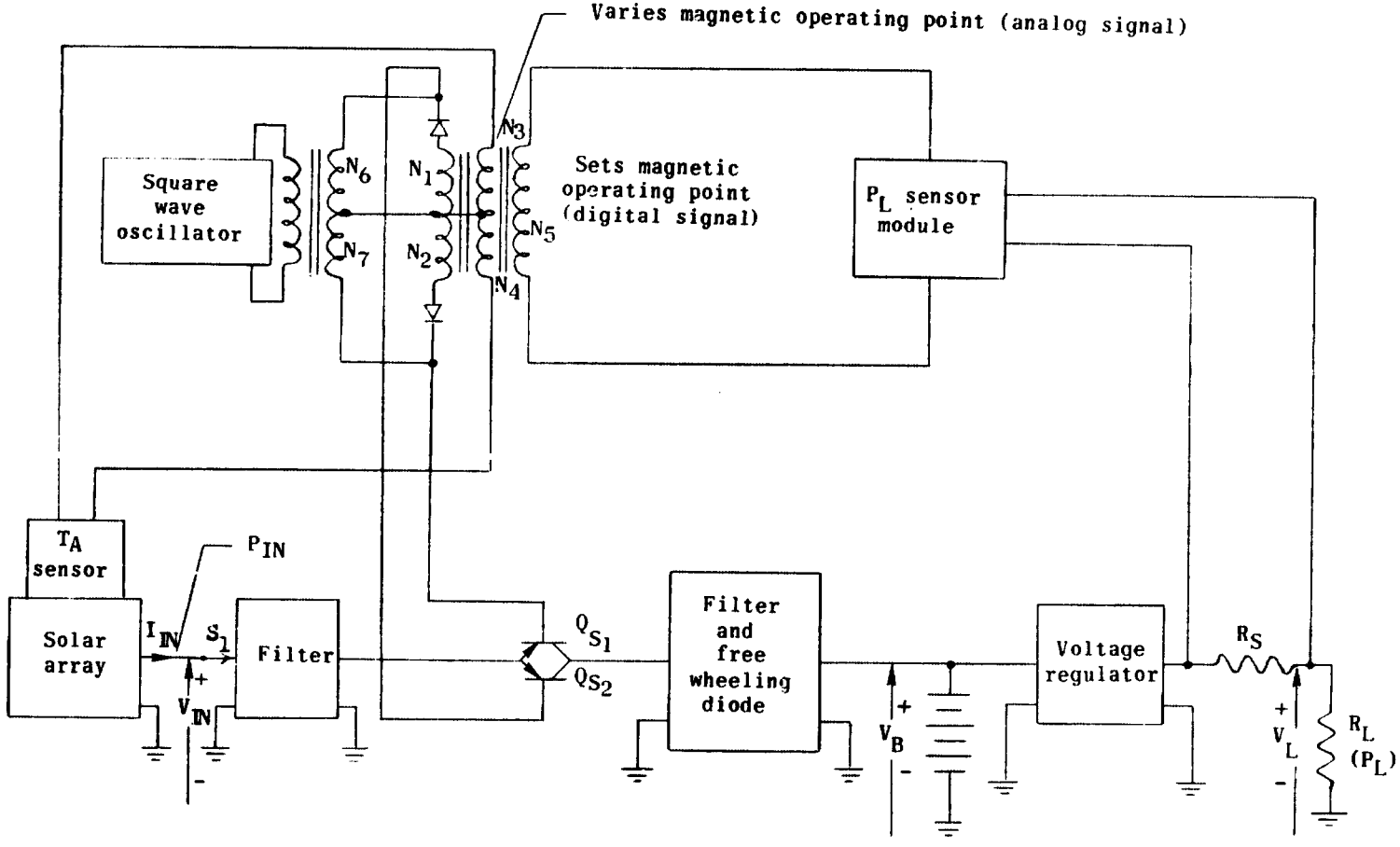

Figure 18.- A candidate for the taper-current battery-charge system.

physically mounted with the power generating solar cells of the array. Hence, nominally speaking, the temperature of each of the solar cells, including the T_A sensor solar cell, would be the same. Of course, the T_A sensor solar cell would be electrically isolated from the power generating solar cells. The T_A sensor solar cell and its windings (N_3 and N_4) could be calibrated versus array temperature in an open loop manner. If the individual solar cell, N_3 and N_4 arrangement was not sensitive enough for the application, then the individual solar cell could be replaced by a module of series and/or parallel connected solar cells. The number of series and/or parallel connected T_A solar cells would depend on the sensitivity and possibly dynamics of the T_A sensor loop.

The experiment power sensor module senses a low valued signal across the experiment power sensing resistor (R_S). R_S would be of very low value, perhaps 0.1 ohm. The P_L sensor module could perhaps be a transistorized inverter, which has two possible output states. The output inverter state would depend on whether $P_L = P_{L_{max}} = 56$ w or $P_L = P_{L_{min}} = 28$ w. The P_L sensor module determines the quiescent operating point by controlling which of two current values flows through its winding N_5.

The two filters, in the main power path, decreases the ripple and interference reflected towards the load and source by the switching action of Q_{S_1} and Q_{S_2}.

A practical consideration for the TCC would be the choice of the value for the switching frequency (f_S). A choice of a value for

f_S implies a compromise between TCC efficiency (EFF_T) and filter component size. By increasing f_S, the required filter values decrease, which means smaller filter subassemblies. However, as f_S increases, the switching power losses of Q_{S_1} and Q_{S_2} increase, as well as increased core losses. Therefore as f_S is increased EFF_T decreases. A typical range of f_S for an application as shown in Figure 18 would be 1.0 to 10.0 K.C.

CHAPTER VII

EXPERIMENTAL RESULTS

There was a small amount of experimental work done for this thesis. The experimental results are not conclusive but rather serve to give general evidence to the practical nature of a TCS.

Various types of test equipment were utilized to gather the experimental data. A solar array simulator, designed by the Neotec Corporation,[2] was used as the source of power instead of an actual solar array. This is a convenient substitution, since a solar array would require an intense light source with an optical focusing system. A differential voltmeter, manufactured by the John Fluke Co., was used for all dc voltage measurements. Weston Ammeters were used for all dc current measurements. A Tektronix oscilloscope was used to monitor the τ of the TCC in the TCS. Two Trygon dc power supplies were utilized to simulate the T_A sensor and P_L sensor control signals.

The first step in gathering the empirical data was to generate solar array simulator current versus voltage reference curves. In order to generate these curves, it is first necessary to properly set-up the controls of the solar array simulator. The current versus voltage reference simulator curves were generated by the test set-up

---

[2]Technical Manual for Solar Array Simulator, Model N66-455W, Neotec Corporation, Rockville, Md.

shown in Figure 19. The resulting four reference curves are shown in Figure 20. Note from Figure 20 that each curve has the same nominal I_{sc} but a different V_{oc} value. An I_{sc} value of 1.0 amp was chosen since it is compatible with the current limitations of the TCC utilized in the empirical work.

For each reference curve of Figure 20, the value of V_P was determined by trial and error. The locus of P_A is shown in Figure 20. The value of V_P for each curve serves as a reference in the performance of the TCC.

Figure 21 indicates the test set-up utilized for the TCS. The TCC that was actually used is essentially the saturable core reactor circuit shown in Figure 18. The TCC receives the power from the solar array simulator and also a pair of dc voltages from two dc power supplies. One power supply simulates the T_A sensor signal (V_T), whereas the other supply simulates the P_L sensor signal (V_E).

The following was the philosophy employed while taking data with the set-up of Figure 21. Two values of R_L were used: 20 ohms and 40 ohms, the former value representing $P_{L_{max}}$ and the latter representing $P_{L_{min}}$. Note from Figure 21 that the voltage regulator discussed throughout the thesis is absent. At the time this laboratory work was done, a suitable voltage regulator was not available. Hence, the resulting $P_{L_{max}}$ and $P_{L_{min}}$ was not of a two-to-one ratio as was used in the thesis description. In the data collection, first $R_L = 20$ ohms was used. The ideal situation is that for each reference curve of the solar array simulator, V_T be adjusted such that $V_{IN} = V_P$

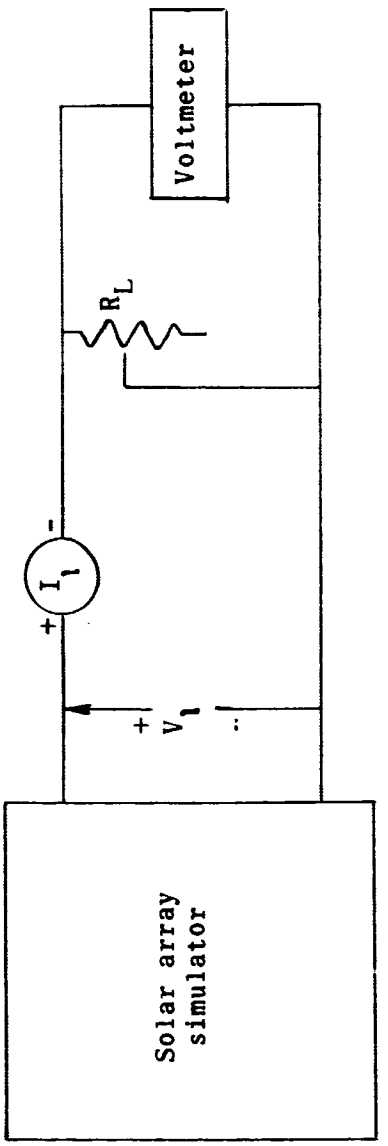

Figure 19.- Test set-up utilized to obtain solar array simulator reference curves.

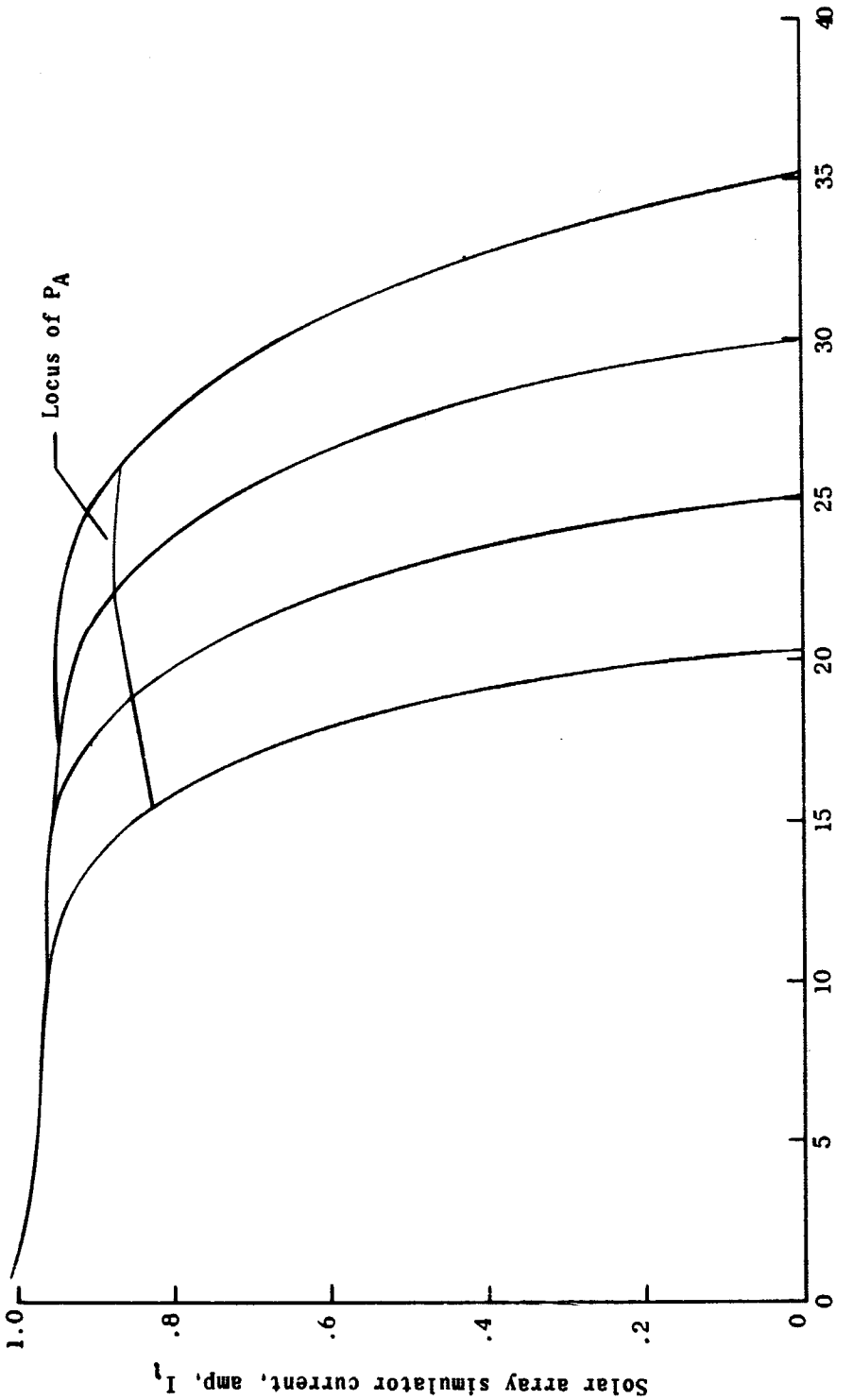

Figure 20.- Solar array simulator reference curves.

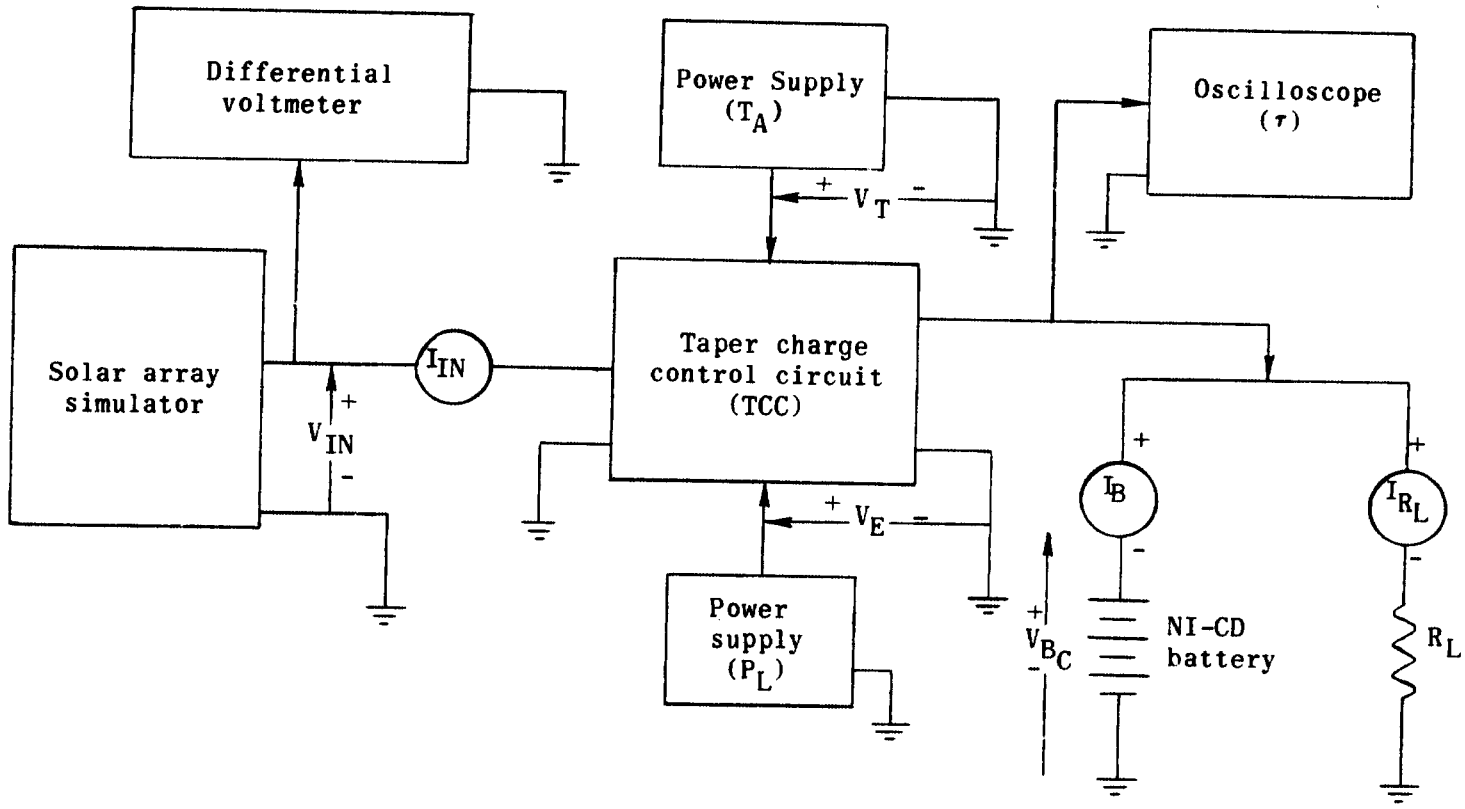

Figure 21.- Block diagram of test set-up for empirical data of taper-current battery-charge system.

for that particular curve (matched case). However, the ideal situation was not achieved. The entire set of data collected is shown in Table I.

Note from Table I, for R_L = 20 ohms, that $V_{IN} \neq V_P$ but was only made to approach the V_P value for each of the four curves. Observe the I_{B_C} data of Table I, which serves as the key to the mismatching philosophy employed in the data collection. It was decided that, for R_L = 40 ohms, V_T be adjusted for each simulator reference curve such as to produce the same I_{B_C} value as for R_L = 20 ohms. This mismatching philosophy is essentially the same as described in the body of this thesis.

Observing Table I there exists a gross discrepancy. For the case of R_L = 20 ohms, $P_{IN} > P_A$ for each of the four reference curves. This is impossible since P_A is the maximum available power for each curve. This discrepancy can perhaps be explained by malfunction and/or drift of the solar array simulator. Note from Table I that V_E was adjusted for a constant value for R_L = 20 ohms and another for R_L = 40 ohms. Due to the omission of the voltage regulator, P_L varied for a given constant value of R_L. The EFF_T remained high regardless of the value of R_L and regardless of which reference simulator curve was used. Figure 22 shows the variation of τ versus V_{oc}, taken from the data in Table I. Since V_{oc} is linearly proportioned to T_A over a wide T_A range, curves similar to those in Figure 22 describe τ versus T_A. Figure 22 is based on the measured value of

Table I.- Empirical Data for Taper-Current Battery-Charge System

Ⓐ R_L = 20 ohms ; V_E = 0.25 vdc

V_{oc} (vdc)	V_p (vdc)	V_{IN} (vdc)	I_{IN} (mA)	P_{IN} (w)	P_A (w)	V_{B_C} (vdc)	I_{R_L} (mA)	I_{B_C} (mA)	EFF_T (%)	(Meas.) τ (%)	(Cal.) τ (%)	V_T (vdc)
20.0	15.5	16.3	881	14.36	12.7	16.2	808	59.2	97.7	100	99.4	3.41
25.0	19.0	21.2	860	18.22	15.93	17.2	871	130	95.3	81.6	81.2	3.43
30.0	22.25	26.9	750	20.20	19.16	18.0	875	146	90.8	68.4	67.0	3.52
35.0	26.25	31.5	860	27.08	22.3	20.0	970	286	92.4	65.3	63.4	3.76
Ⓑ R_L = 40 ohms ; V_E = 0.40 vdc												
20.0	15.5	18.8	439	8.25	12.7	16.9	411	59.2	96.8	88.8	89.8	3.37
25.0	19.0	23.7	455	10.8	15.93	18.1	440	130	95.6	67.3	76.4	3.43
30.0	22.25	28.8	409	11.8	19.16	18.3	447	146	91.5	73.4	63.5	3.53
35.0	26.25	33.8	511	17.28	22.3	20.4	498	286	92.4	70.5	60.4	3.68

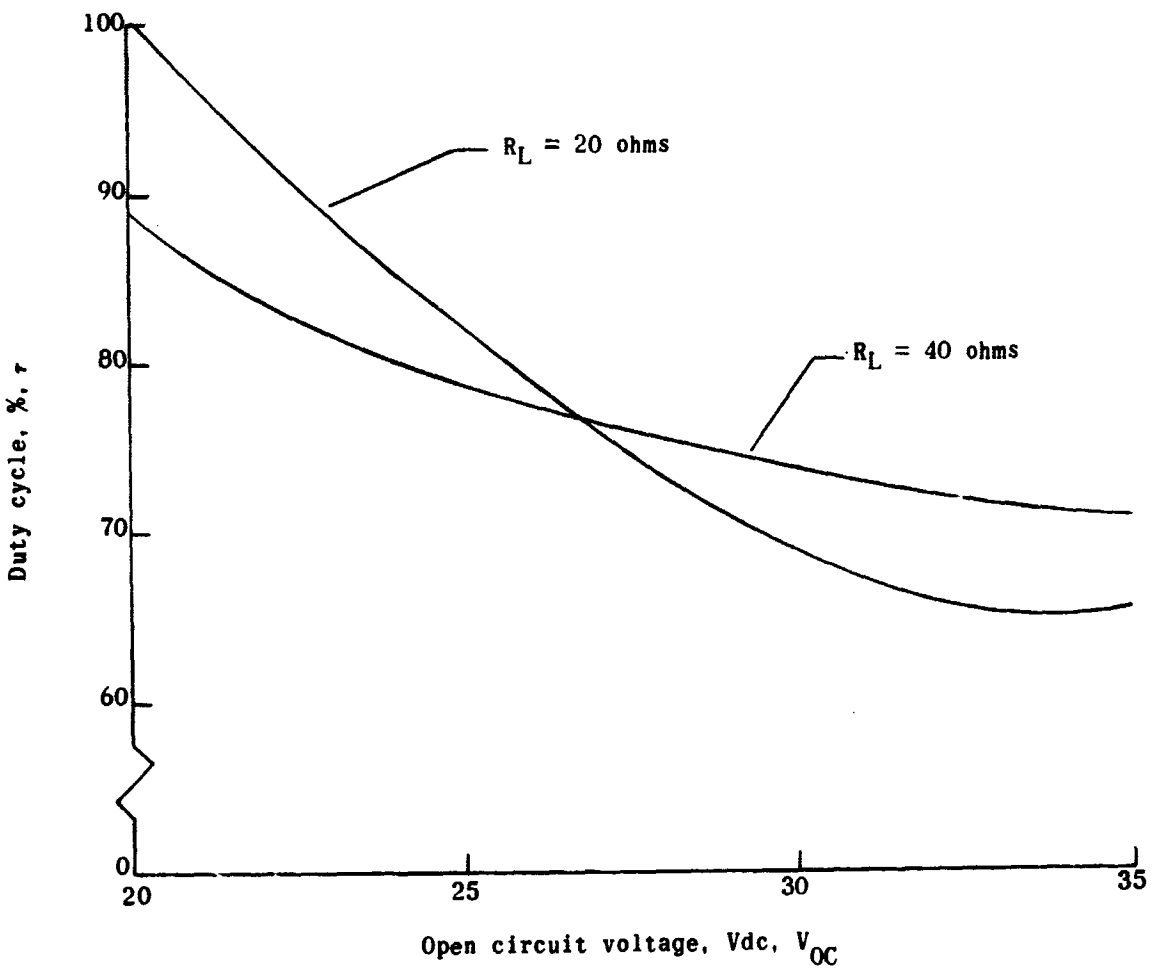

Figure 22.- Duty cycle (measured) vs. open circuit voltage for taper-current battery-charge system.

τ as opposed to its calculated value. In this figure the τ at V_{oc} = 25 vdc and R_L = 40 ohms was "out of line" with the rest of the curve, hence it was ignored. Perhaps this point was in error due to a false oscilloscope reading of τ. Figure 23 represents τ versus V_{oc}; this figure is based on the calculated τ value. The curves of Figure 23 are those that one would expect for a TCS, since the curves are smooth and do not cross.

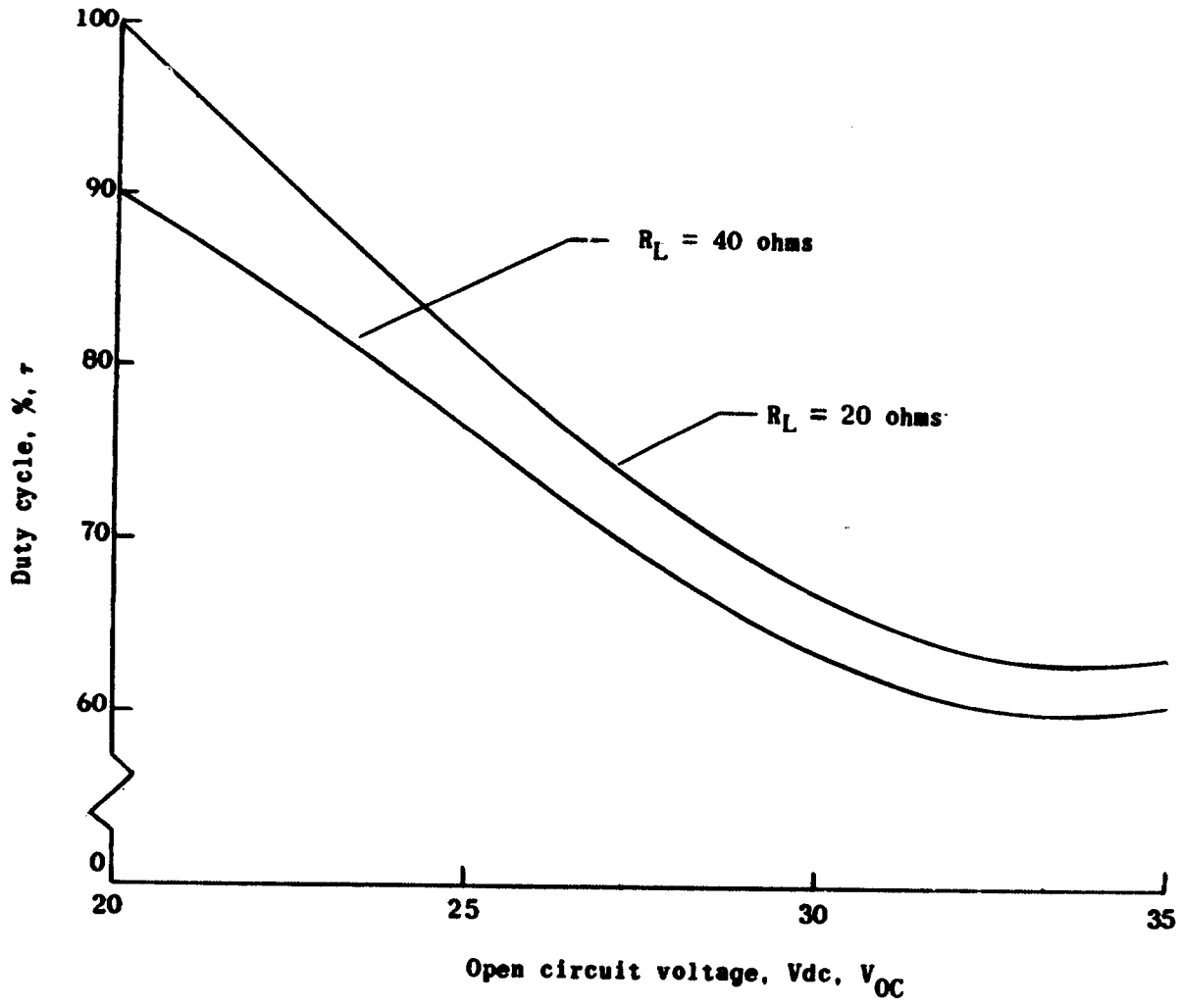

Figure 23.- Duty cycle (calculated) vs. open circuit voltage for taper-current battery-charge system.

CHAPTER VIII

CONCLUSIONS

A method of designing a near-optimum solar array for an orbiting spacecraft has been given. The optimization is produced by constraining the solar array to operate at its maximum power point over the full array temperature range as long as the condition of maximum experiment power demand exists. If the experiment power demand decreases, then the solar array is mismatched from the point of maximum power. Essentially this mismatch in solar array power is equal to the decrease in experiment power.

The control in the solar array operating point results in producing a taper charge current versus array temperature for the orbiting spacecraft storage battery. The constraintment of solar array operating point and associated taper battery charging results is a solar array that is least expensive, lowest in weight, and smallest in area for a given array power requirement. The savings in solar array cost, weight, and area are shown by comparing a taper-current battery-charge system to a constant-current battery-charge system. The comparison is made on the basis of the same mission constraints, such as the same orbit characteristics and experimented power demands.

A small amount of laboratory work was done to become familiar with the practical problems of the taper battery-charge system. A solar array simulator was utilized instead of an actual physical solar

array. The resulting data were insubstantial, but leads one to suspect the practical possibilities of the proposed power system.

BIBLIOGRAPHY

BIBLIOGRAPHY

Honeywell, Inc., Systems and Research Division, "A Proposal for Design and Development of Adaptive Power Conditioning for Solar Cell Energy Sources," Minneapolis, Minnesota, January 1965.

Hughes Aircraft Co., Research and Development Division, Aerospace Group, Final Report on the "Nondissipative Solar Array Optimum Charge Regulator," Culver City, California, July 1966.

Ross, B., "Design Criteria for Satellite Power Supplies Using Radiation Resistant Solar Cells" Semiconductor Division of Hoffman Electronics Corp. El Monte, California, March 1963.

Geyger, W. A., "Nonlinear-Magnetic Control Devices," McGraw Hill Book Co., Inc., 1964.

The Engineering Staff of Texas Instruments Inc., "Transistor Circuit Design," McGraw Hill Book Co., Inc., 1963.

Motorola Switching Transistor Handbook, July 1966.

Motorola Power Transistor Handbook, First Edition, 1961.

Neotec Corp., "Technical Manual for Solar Array Simulator," (Model N66-455 w), Rockville, Maryland, 1966.

Quality Evaluation Laboratory, "Evaluation Program for Secondary Spacecraft Cells" - Second Annual Report of Cycle Life Test - Nad Crame, Indiana.

APPENDIX

APPENDIX I

Derivation of:

$$\tau = \frac{V_{B_C}}{V_{IN}} \times 100$$

The following figure aids in the development of this derivation:

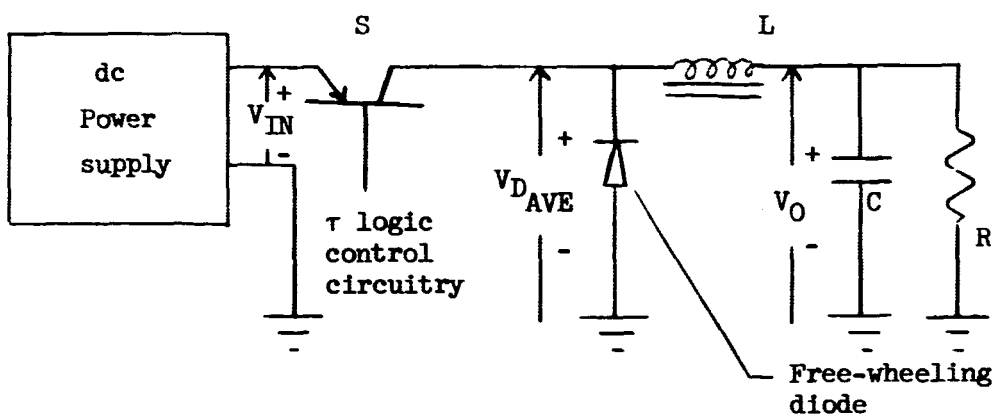

Figure (A-1).- Duty cycle derivation sketch.

In the above figure, S represents the electronic power switch of the TCC. S is switched at a constant frequency (f_S) by the τ logic control circuitry. The variable in the switching action is the on time (T_{ON}) per switching period (T_S) of S.

Essentially, the derivation rests on proving that

$$\tau = \frac{V_{D_{AVE}}}{V_{IN}} \times 100 \qquad \text{(A-1)}$$

where $V_{D_{AVE}}$ is the average dc voltage as measured across the free-wheeling diode, and V_{IN} is the dc input voltage of the power supply in Figure (A-1).

The output dc voltage (for the experiments) V_O is equal to $V_{D_{AVE}}$ less the very small dc voltage drop across the filter choke (L). Hence, once Equation (A-1) is proven, we can essentially say that

$$\tau = \frac{V_O}{V_{IN}} \times 100 \tag{A-2}$$

Once Equation (A-2) is proven, V_O can be replaced by V_{B_C} (battery charge voltage), and the V_{IN} of the dc power supply can be replaced by the V_{IN} of a solar array. These substitutions lead to

$$\tau = \frac{V_{B_C}}{V_{IN}} \times 100 \tag{A-3}$$

which would complete the derivation.

The average dc voltage across the free-wheeling diode can be represented as in Equation (A-4)

$$V_{D_{AVE}} = \frac{1}{T_S} \int_o^{T_S} v_D \, dt \tag{A-4}$$

where v_D is the instantaneous free-wheeling diode voltage drop.

$$T_S = T_{ON} + T_{OFF} \tag{A-5}$$

Hence,

$$V_{D_{AVE}} = \frac{1}{T_S}\left[\int_o^{T_{ON}} v_D \, dt + \int_{T_{ON}}^{T_S} v_D \, dt\right] \tag{A-6}$$

Let it be assumed that both the electronic power switch and the free-wheeling diode act as perfect push-pull switches. That is to say that

during $0 < t \leq T_{ON}$, the electronic power switch is conducting and has zero forward resistance, and the free-wheeling diode is open and has infinite back resistance. During $T_{ON} < t \leq T_S$, the electronic power switch is open and has infinite resistance, and the free-wheeling diode is closed and has zero forward resistance. With these assumptions in mind, we can state mathematically,

$$V_{D_{AVE}} = \frac{1}{T_S}\left[\int_o^{T_{ON}} (V_{IN})dt + \int_{T_{ON}}^{T_S} (0)dt\right] \tag{A-7}$$

$$V_{D_{AVE}} = \frac{V_{IN}}{T_S} \int_o^{T_{ON}} dt \tag{A-8}$$

$$V_{D_{AVE}} = \frac{V_{IN}}{T_S} T_{ON} \tag{A-9}$$

and so

$$\frac{T_{ON}}{T_S} = \frac{V_{D_{AVE}}}{V_{IN}} \tag{A-10}$$

It is defined that

$$\tau = \frac{T_{ON}}{T_S} \tag{A-11}$$

Consequently,

$$\tau = \frac{V_{D_{AVE}}}{V_{IN}} \tag{A-12}$$

As can be seen in Figure (A-1), V_O is approximately equal to $V_{D_{AVE}}$ since the dc voltage drop across the filter choke will be very small (perhaps 0.5 volt).

Hence,

$$\tau = \frac{V_O}{V_{IN}} \tag{A-13}$$

For the taper-current battery-charge system, $V_O = V_{B_C}$. Therefore,

$$\tau = \frac{V_{BC}}{V_{IN}} \tag{A-14}$$

To express τ in percent,

$$\tau = \frac{V_{BC}}{V_{IN}} \times 100 \tag{A-15}$$

This completes the desired derivation.

In the preceding derivation it was assumed that both the electronic power switch and the free-wheeling diode act as perfect switches. The validity of the assumption of these switches behaving as perfect open circuits during their respective off times depends on their associative leakage currents. The electronic power switch and the free-wheeling diode are each semiconductor components. Leakage current in semiconductors can become a protlem if their temperatures become abnormally high. By proper heat sink design, excessive semiconductor temperatures can be avoided. The validity of the assumption that the switches behave as perfect short circuits during their respective on

times depends on their associative saturation voltage drops. The typical range of saturation voltage for a semiconductor switch is from 0.05 to 0.75 vdc, depending on semiconductor component quality and level of power being switched. In this thesis a power of either 56 w or 28 w was switched, so a saturation voltage of 0.50 vdc was arbitrarily chosen as a typical value. In this derivation the assumption of a perfect switch also assumes that both the electronic power switch and freewheeling diode make their associative switching actions in zero time. Hence, delay time, rise time, storage time, and fall time are each assumed to be nonexistent for both switches.